Geoscience Frontiers 17 (2026) 102182

Contents lists available at ScienceDirect

Geoscience Frontiers

journal homepage: www.elsevier.com/locate/gsf

Research Paper

First evidence of ca. 1.77 Ga S-type magmatism, Aravalli orogen: Implications for the late Paleoproterozoic geodynamic evolution of NW India

Parampreet Kaur [a,*], Armin Zeh [b,c], Naveen Chaudhri [a], Prabhakar Dutta [a], Swati Sharma [a]

[a] Department of Geology, Panjab University, Chandigarh 160 014, India
[b] KIT - Karlsruher Institut für Technologie, Campus Süd, Institut für Angewandte Geowissenschaften, Mineralogie und Petrologie, Adenauerring 20b, Geb. 50.4, D-76131 Karlsruhe, Germany
[c] Frankfurt Isotope and Element Research Center (FIERCE), Goethe-University Frankfurt, D-60438 Frankfurt am Main, Germany

ARTICLE INFO

Article history:
Received 30 July 2025
Revised 2 October 2025
Accepted 10 October 2025
Available online 16 October 2025

Keywords:
Aravalli orogen
Late Paleoproterozoic
S-type granites
syn-collisional magmatism
Zircon U-Pb-Hf isotopes
Columbia supercontinent

ABSTRACT

Present models for the late Paleoproterozoic evolution of the Aravalli orogen (NW India) postulate the existence of a continental magmatic arc active between 1875 Ma and 1810 Ma, followed by a phase of post-collisional magmatism between 1730 Ma and 1700 Ma. However, the tectono-magmatic processes occurring between these two events remain cryptic. In this study, evidence for an intervening magmatic phase is revealed based on the investigation of granitoids exposed in the southern part of the Aravalli orogen. U-Pb zircon dating of these granitoids (granites to tonalites) yielded emplacement ages between 1770 Ma and 1760 Ma. Whole-rock geochemical data indicate a strongly peraluminous, S-type, high-K calc-alkaline character, with magnesian to ferroan signatures and a *syn*-collisional tectonic affinity. The REE patterns are predominantly highly fractionated, displaying depleted HREE profiles and moderate to weak negative Eu anomalies. The geochemical data further suggest derivation of the granitoids by partial melting of *meta*-greywackes at temperatures > 800 °C. Subchondritic $\varepsilon_{Hf}(t)$ values (−11.0 to −2.6) further indicate reworking of a heterogeneous crust. The results of this and previous studies collectively indicate that the Aravalli orogen evolved through three distinct late Paleoproterozoic tectono-magmatic phases: (1) subduction-related magmatism at 1875 1810 Ma, (2) *syn*-collisional S-type plutonism at ca. 1770 Ma, and (3) post-collisional extension-related A-type magmatism at ca. 1720 Ma. Globally, Paleoproterozoic S-type granites were predominantly derived by anataxis of Archean crust. Additionally, the data suggest that the northern margin of proto-India collided with fragments of the Columbia supercontinent at ca. 1770 Ma, postdating Columbia's maximum packing time (1900–1850 Ma).

1. Introduction

Granitoids constitute one of the most widely distributed components in the Earth's continental crust, particularly in Precambrian terrains (Patiño Douce, 1999; Condie, 2011). The magma composition of these rocks is primarily controlled by pressure, temperature and source rock. These variables of magma generation are further controlled by the tectonic regime (Collins et al., 2020). The granitoids associated with subduction, collision and post-collision settings provide crucial insights into the geodynamic processes controlling the evolution of continents (Zhang et al., 2019; Song et al., 2022). Based on the magma source characteristics, granitoids are mostly discriminated as I-type and S-type (Chappell and White, 1974, 2001). The strongly peraluminous S-type granites (aluminium saturation index > 1.1; Bucholz et al., 2018) typically occur in continental collision zones (Barbarin, 1999; Zhu et al., 2020), but also form in various tectonic settings, such as back-arc extension (Collins and Richards, 2008), ocean-ridge subduction (Hildebrand et al., 2010) and post-collision (Sylvester, 1998). These granitoids are predominantly formed by the anatexis of metasedimentary rocks in the middle-lower continental crust induced either by decompression of over-thickened continental crust or advection/conduction of mantle-derived heat into the lower crust (White and Chappell, 1988; Sylvester, 1998; Villaseca et al., 1998; Barbarin, 1999; Chappell and White, 2001; Bucholz and Spencer, 2019; Nabelek, 2020).

* Corresponding author.
E-mail address: param.geol@gmail.com (P. Kaur).

https://doi.org/10.1016/j.gsf.2025.102182

The mechanism responsible for the generation of *syn*-collisional granitoids is, however, not always straightforward because the process of collision is a geotectonic concept and is highly dynamic, progressing through pre-collisional, *syn*-collisional (initial to ongoing), and to a post-collisional phase (Harris et al., 1986; Zhu et al., 2015; Song et al., 2022). Thus, combined results of geochronology and geochemistry are required to constrain *syn*-collisional phase of magmatism in an orogenic belt. Moreover, collision-related magmatism is a key indicator of the mature stages of supercontinent assembly (Şengör and Natal'in, 1996; Cawood et al., 2009).

The Aravalli orogen, located in the North Indian Block (Fig. 1a), preserves evidence of 1875–1810 Ma Andean-style continental arc magmatism (Kaur et al., 2009, 2017a, 2023a), and a phase of post-collisional extensional magmatism at 1730–1700 Ma (Fig. 1b; Kaur

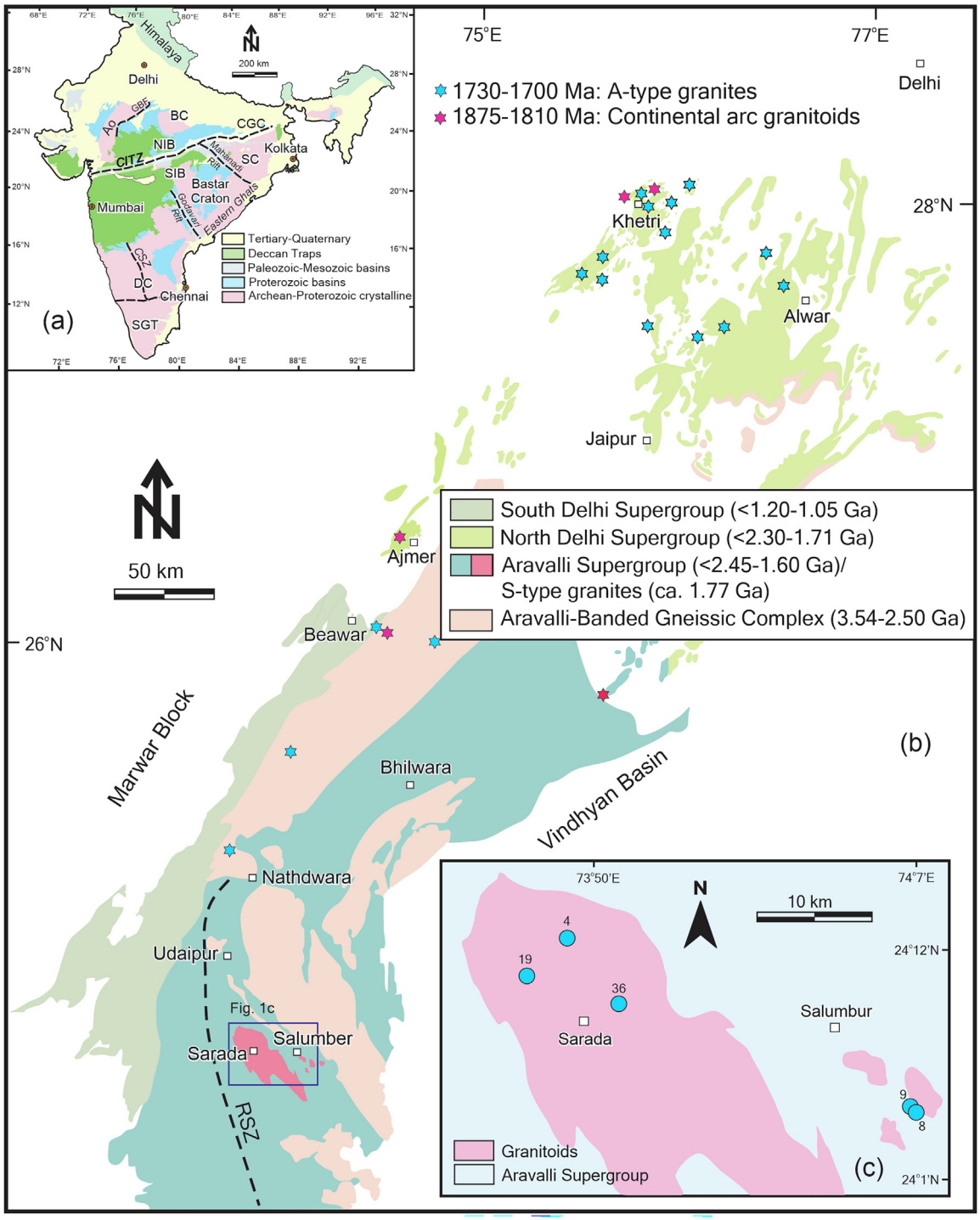

Fig. 1. (a) Geological map of India, showing various crustal blocks (Colleps et al., 2021 and references therein) and (b) regional geological map of the Aravalli orogen, northwest India, showing prominent Precambrian stratigraphic units and location of the study area (compiled from Heron, 1923; Das, 1988; Singh, 1988; Gupta et al., 1997; Roy and Jakhar, 2002; Kaur et al., 2015, 2017a) and (c) geological maps of the Sarada and Salumbar granitoids, showing locations of analysed samples (after Gupta et al., 1997); Prefixes for the sample numbers are omitted to avoid crowding and correspond to those provided in Table 2. RSZ: Rakhabdev Shear Zone, NIB: North Indian Block, SIB: South Indian Block, GBF: Great Boundary Fault, CITZ: Central Indian Tectonic Zone, CGC: Chotanagpur Gneissic Complex, CSZ: Chitradurga Shear Zone, SGT: Southern Granulite Terrane, Ao: Aravalli orogen, BC: Bundelkhand Craton, DC: Dharwar Craton and SC: Singhbhum Craton.

et al., 2017b, 2017c, 2021, 2025; Pandit et al., 2021; Ahmad et al., 2023). However, evidence for an intervening collisional phase remains elusive. Currently, only cryptic indicators exist, such as ca. 1765 Ma zircon xenocrysts in granitoids and detrital zircon grains of 1770–1750 Ma in metasedimentary rocks of the Aravalli orogen (Kaur et al., 2011a, 2017c, 2019a).

In this study, we present a new combined dataset, comprising zircon U-Pb ages, Lu-Hf isotopic compositions, and whole-rock geochemical data from granitoids exposed in the southern Aravalli orogen. These results not only provide new constraints on the geodynamic evolution of the Aravalli orogen during the late Paleoproterozoic, but also help in redefining the lithostratigraphic position of the southern Aravalli-Banded Gneissic Complex (Aravalli-BGC), which has long been considered an exclusively Archean terrane, lacking evidence of post-Archean magmatic events. Furthermore, the new results also have important implications for reconstructing the assembly of the Columbia supercontinent.

2. Geological framework

The Aravalli-BGC (3.54–2.50 Ga) forms a cratonic nucleus in northwestern India and is overlain by three Paleo- to Neoproterozoic supracrustal units (Fig. 1b). These comprise the Aravalli Supergroup, the North Delhi Supergroup and the South Delhi Supergroup, deposited at < 2.45–1.60 Ga, <2.30–1.71 Ga and < 1.20–1.05 Ga, respectively (Kaur et al., 2011a, 2013a, 2019a, 2022, 2023b; McKenzie et al., 2013; Wang et al., 2017, 2019). In the east and southeast of Udaipur city, rocks of the southern Aravalli-BGC are exposed (Fig. 1b) and are unconformably overlain by the Aravalli Supergroup (Roy and Jakhar, 2002).

The southern Aravalli-BGC is a granite-greenstone terrane, composed largely of Paleoarchean tonalite-trondhjemite-granodiorite (TTG) gneisses (ca. 3310 Ma), and Neoarchean metabasites (ca. 2828 Ma), TTGs (2565–2550 Ma), sanukitoids (ca. 2540 Ma) and potassic granitoids (2560–2500 Ma), with evidence of later metamorphic overprints at ca. 2450 Ma and 520 Ma (Gopalan et al., 1990; Upadhyaya et al., 1992; Wiedenbeck and Goswami, 1994; Roy and Kröner, 1996; Wiedenbeck et al., 1996; Mondal and Raza, 2013; Rahaman and Mondal, 2015; Kaur et al., 2019b; Dutta et al., 2025). Field observations suggest (Heron, 1953; Gupta et al., 1997; Roy and Jakhar, 2002) that some of these potassic granitoids occur as inliers within the metasedimentary rocks of the Aravalli Supergroup (e.g. Sarada; Fig. 1b), form part of an Archean basement or even intrude the rocks of the Aravalli Supergroup (e.g. Salumbar; Fig. 1b). Consequently, the stratigraphic status of these potassic granitoids remains ambiguous.

The term "Sarada inlier" is well entrenched in the geological literature of the Aravalli orogen. Heron (1953) coined the term Sarada inlier and considered these rocks equivalent to those of the Aravalli-BGC. Gupta et al. (1997) identified an erosional unconformity between the rocks of the Aravalli Supergroup and those of the pre-Aravalli Sarada inlier. The lithology of the Sarada inlier includes composite gneisses, metapelites, and thin bands of marble and quartzite (Gupta et al., 1997). No precise geochronological constraints are available for the Sarada rocks, although Crawford (1970) reported a minimum Rb-Sr model age of ca. 1840 Ma for the Sarada granite.

The granitoids located about 4 km southeast of Salumbar are exposed as four major isolated plutons (Fig. 1b). They are interpreted either as part of the southern Aravalli-BGC (Roy and Jakhar, 2002), post-Aravalli intrusives (Gupta et al., 1997) or post-lower Aravalli intrusives (Shekhawat et al., 2001). Presently, no precise age data are available for these granitoids to support these contentions.

3. Samples and analytical methods

Five representative samples were selected for whole-rock geochemical and combined U-Pb-Hf isotope analyses, including three from the Sarada granitoids and two from the Salumbar granitoids. Sample coordinates are given in Table 1, and their locations are shown in Fig. 1c.

The whole-rock geochemical data were analysed at Activation Laboratories, Ontario, Canada, using a fusion method with a flux of lithium metaborate and lithium tetraborate (package: WRA 4B2 + 4Litho). Analytical details are provided in Hoffman (1992) and at https://www.actlabs.com.

The sample preparation method for zircon grains used in combined U-Pb-Hf isotope analyses is briefly outlined in electronic (Supplementary Data Table S1), with detailed procedure described in Kaur et al. (2023a). Uranium-Pb analyses were conducted using a laser ablation-sector field-inductively coupled plasma-mass spectrometer (LA-SF-ICP-MS) with a 193 nm ArF Excimer laser (Analyte Exite+, Teledyne Photon machines) coupled to Thermo-Scientific Element XR instrument at the Karlsruhe Institute of Technology, Karlsruhe, Germany. Raw data were corrected offline using an in-house MS Excel© spreadsheet program (Gerdes and Zeh, 2006, 2009).

Lutetium-Hf isotope analyses were performed using a Resolution M-50 193 nm ArF Excimer laser system coupled to a Thermo-Scientific multicollector (MC)-SF-ICP-MS (Neptune) at Goethe University of Frankfurt, Germany. The analytical protocols follow those described in Gerdes and Zeh (2006) and Zeh and Gerdes (2012 and references therein). Detailed operating conditions for U-Pb dating and Lu-Hf isotope analyses are given in Supplementary Data Table S1. Results of U-Pb dating and Lu-Hf isotope analyses are summarised in Table 3, and detailed results, including reference material measurements in Supplementary Data Tables S2 and S3.

Additional relevant information and calculation of various parameters for U-Pb and Lu-Hf isotopes are appended in the footnotes of Supplementary Data Table S2 and Table S3, respectively. The ages of the granitoids were calculated using ISOPLOT 3.75 (Ludwig, 2012). All age and Lu-Hf data are reported with 2σ uncertainties, which are the quadratic sum of the within-run precision and the excess of scatter and variance of the secondary reference material.

Table 1
Rock types, locality name, GPS coordinates and mineralogy for analysed samples of the Sarada and Salumbar granitoids.

Sample no.	Locality	Latitude	Longitude	Rock type	Important phases: estimated modal abundances (vol.%)
SR-4	Sarada	24°12′7.00″N	73°48′17.56″E	Tonalite	Qz 30%, Pl 19%, Bt 24%, Ms 19%, Grt 7%, Kfs 1%
SR-19	Sarada	24°10′36.30″N	73°46′41.30″E	Tonalite	Pl 51%, Qz 32%, Bt 13%, Kfs 3%, Ms 1%
SR-36	Sarada	24°9′4.20″N	73°51′09.70″E	Granite	Qz 30%, Kfs 32%, Pl 18%, Bt 13%, Ms 4%, Grt 2%
2NG-8	Salumbar	24°38′17.7″N	74°03′48.2″E	Tonalite	Pl 37%, Qz 31%, Bt 20%, Ms 7%, Acc. 5%
2NG-9	Salumbar	24°46′06.9″N	74°29′06.6″E	Granite	Qz 36%, Pl 27%, Kfs 26, Bt 4%, Ms 2%, Acc. 5%

Mineral abbreviations are after Whitney and Evans (2010). Acc.: Accessory minerals.

4. Results

4.1. Petrography

Texturally, the Sarada granitoids are foliated, medium- to coarse-grained, and vary from porphyritic (sample SR-4; Fig. 2a and b) to equigranular (SR-36; Fig. 2c). At places, these rocks show migmatite-like structures (sample SR-19; Fig. 2d). Mineralogically, they can be classified either as tonalite or granite *sensu stricto* (Fig. 3a and Table 1). The tonalites mainly consist of plagioclase, quartz and biotite, but also contain variable amount of primary muscovite and minor K-feldspar (Fig. 2e). The granite comprises quartz, K-feldspar, plagioclase and biotite as major minerals, with primary muscovite occurring as a minor phase (Fig. 2f). Notably,

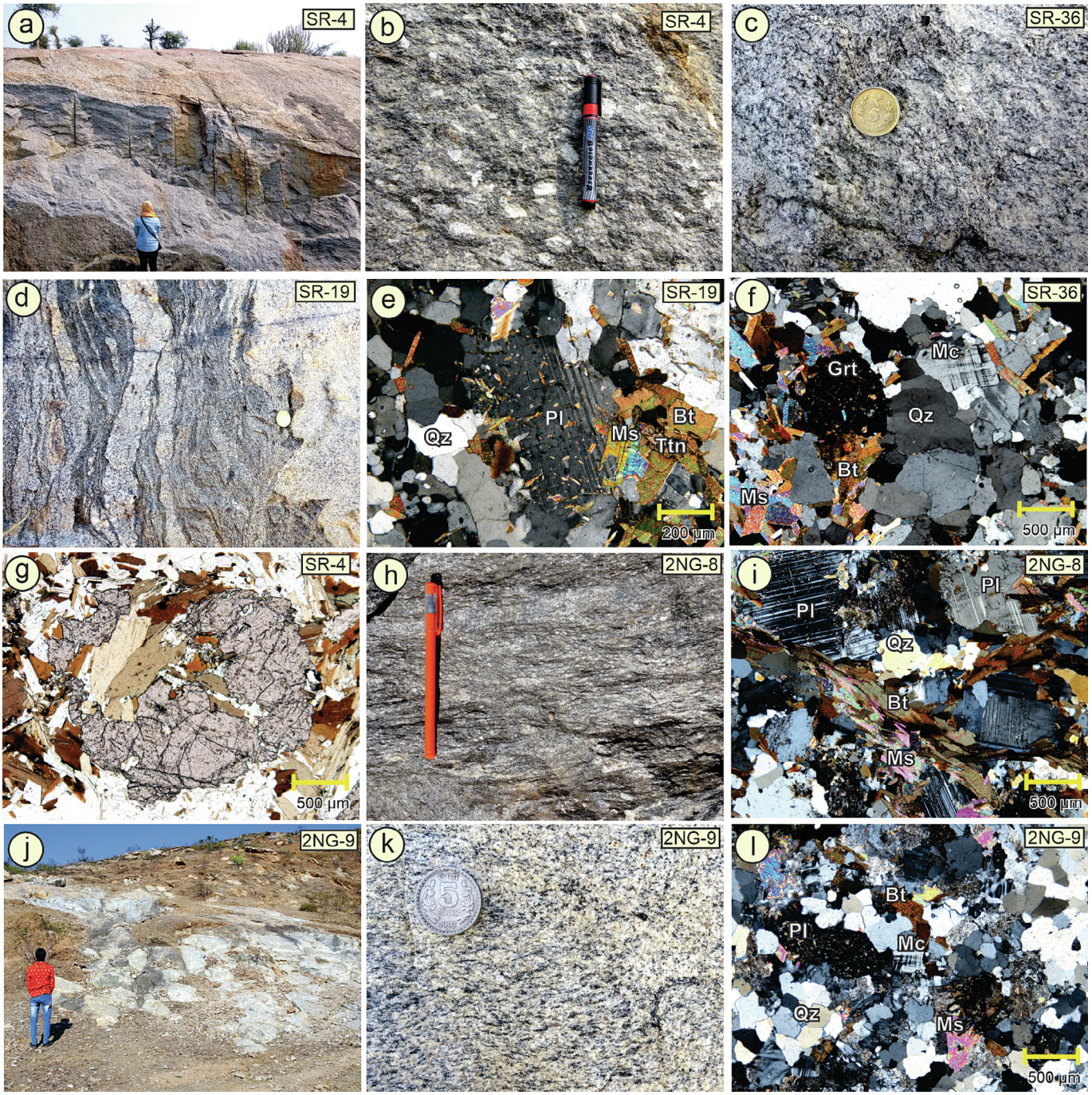

Fig. 2. Representative field photographs and photomicrographs of the Sarada and Salumbar granitoids. Photomicrograph (g) is taken under plane polarised light and all others are under crossed nicols. (a) Overall outcrop view of the Sarada tonalite, (b) same tonalite, showing porphyritic nature, (c) Sarada granite displaying an equigranular fabric, (d) Sarada tonalite, showing a migmatitic-like structure, (e) overall view of the Sarada tonalite, showing its main mineralogy and texture, (f) an overall view of the Sarada granite, (g) occurrence of garnet in the Sarada tonalite, (h) overall view of the Salumbar tonalite, showing a porphyritic texture, (i) thin section view of the Salumbar tonalite, illustrating its texture and mineralogy, (j) outcrop view of the Salumbar granite, (k) close-up of the same outcrop, showing an equigranular texture and (l) overall view of the same rock type, showing its main mineralogy and texture. Bt: Biotite, Grt: Garnet, Mc: Microcline, Ms: Muscovite, Pl: Plagioclase, Ttn: Titanite and Qz: Quartz (after Whitney and Evans, 2010). GPS coordinates for sample locations are same as mentioned in Table 1.

both the tonalites and granite contain small amounts of garnet (Fig. 2g), as well as accessory tourmaline, apatite, epidote, allanite, zircon, monazite, titanite, calcite and chlorite.

The Salumbar granitoids share similar megascopic characteristics to those of the Sarada granitoids. Like Sarada, they are classified as tonalite or granite (Fig. 3a and Table 1). The tonalite is porphyritic (Fig. 2h) and contains biotite and muscovite as the major mafic phases (Fig. 2i). The granite is equigranular (Fig. 2j and k), with biotite and muscovite present as minor phases (Fig. 2l). Accessory minerals include epidote, titanite, zircon, calcite and chlorite.

4.2. Geochemical characterisation

The Si content in the Sarada granitoids are relatively homogeneous (SiO_2 = 66.8–68.6 wt.%; Table 2), whereas the Salumbar granitoids show more variability (tonalite: SiO_2 = 64.3 wt.% and granite: SiO_2 = 73.1 wt.%; Table 2). Compared to the tonalites, the granites show lower concentrations of Al_2O_3, MgO and CaO (Table 2). All samples are strongly peraluminous, with aluminium saturation index (ASI) values ranging from 1.13 to 1.43 (Fig. 3b and Table 2), except for the Salumbar granite, which is weakly peraluminous (ASI = 1.05). This sample (2NG-9) shows deanorthisation of plagioclase ($An_{1.8}$ to $An_{25.5}$), resulting in a whole-rock loss of Al and Ca and a gain of Na and Si, which leads to a decrease in ASI value (Dutta et al. under preparation). The rocks are predominantly calc-alkalic, high-K calc-alkaline and magnesian to ferroan in nature (Fig. 3c e). The CIPW normative corundum content ranges from 1.79 wt.% to 4.89 wt.%, except for the Salumbar granite (corundum = 0.61 wt.%). These granitoids show an affinity with post-Archean or modern granitoids (Fig. 3f) and can be classified as biotite- and two-mica granites (Fig. 3g).

Furthermore, in the Nb versus Ga/Al discrimination diagram of Whalen et al. (1987), the granitoids do not show an A-type affinity (Fig. 3h) and overlap with both I- and S-type granites. However, their strongly peraluminous nature, reflected by presence of Al-rich minerals (biotite, muscovite and garnet) and CIPW normative corundum (mostly > 1 wt.%) suggest that these are S-type granites (Chappell and White, 1974, 2001; Yang et al., 2019).

The tonalites show fractionated REE patterns [Sarada: $(La/Yb)_N$ = 25.3–43.2 and Salumbar: $(La/Yb)_N$ = 51.9], with depleted HREE profiles [Sarada: $(Gd/Yb)_N$ = 2.8–3.0 and Salumbar: $(Gd/Yb)_N$ = 4.3] and moderate to weak negative Eu anomalies (Eu/Eu^* = 0.57–0.74; Fig. 4a; Table 2). In contrast, the Sarada granite exhibits a less fractionated [$(La/Yb)_N$ = 6.5] and Salumbar granite a highly fractionated [$(La/Yb)_N$ = 102.0] REE pattern. The former displays a flat HREE profile [$(Gd/Yb)_N$ = 1.0] with a moderately negative Eu anomaly (Eu/Eu^* = 0.59; Fig. 4a), while the latter is depleted in HREE ($(Gd/Yb)_N$ = 3.7) showing a strongly negative Eu (Eu/Eu^* = 0.39) anomaly (Fig. 4a). The primitive mantle-normalised multielement patterns for all the granitoids are characterised by pronounced negative anomalies in Nb, P and Ti, as well as in Sr and Eu (Fig. 4b).

4.3. Zircon U-Pb geochronology and Hf isotope compositions

Zircon grains in the Sarada-Salumbar granitoids are primarily euhedral and prismatic, pale pink and transparent. Some grains are colourless to white, translucent to opaque, with rounded to sub-rounded edges (samples SR-4 and 2NG-9). The grains are 80 to 250 μm in length, oscillatory zoned and a few of these show core-rim relationship (Fig. 5a e).

4.3.1. Sarada granitoids

Uranium-Pb spot analyses of Sarada zircon grains provide a wide range of $^{207}Pb/^{206}Pb$ ages from 1431 Ma to 2429 Ma for sample SR-4 (25 spot analyses on 23 grains; Supplementary Data Table S2), 1582 Ma to 1810 Ma for sample SR-19 (25 spot analyses on 24 grains) and 1736 Ma to 2684 Ma for sample SR-36 (25 spot analyses on 23 grains). Most of the analysed zircon domains define upper intercept ages at 1759 ± 7 Ma (sample SR-4; MSWD = 2.2; n = 18), 1768 ± 8 Ma (sample SR-19; MSWD = 1.4; n = 13) and 1767 ± 5 Ma (sample SR-36; MSWD = 0.18; n = 18). These ages are within error identical to their respective concordia ages of 1762 ± 6 (n = 13), 1770 ± 8 (n = 10) and 1768 ± 6 Ma (n = 13) (Fig. 6a, b and c; Table 3) and are interpreted as the crystallisation age of the Sarada granitoids.

A few zircon domains (Th/U = 0.10–1.12) in the analysed samples, with oscillatory zoning mostly provide older concordant ages, ranging from ca. 2684 Ma to 1792 Ma (Fig. 5a, b and c; Table 3), representing xenocrysts. The younger concordant zircon analyses between 1703 Ma and 1749 Ma in sample SR-4, mostly from zircon rims with low Th/U ratios (from 0.04 to 0.14; Supplementary Data Table S2) around older cores (Fig. 5a-v), are most likely metamorphic in origin. Some core domains (Th/U ratios > 0.1) in sample SR-19 with younger $^{207}Pb/^{206}Pb$ ages ranging from 1699 Ma to 1582 Ma (Supplementary Data Table S2), perhaps result from recent Pb-loss.

Most zircon domains yield initial Hf isotope compositions between 0.281508 and 0.281553 (Fig. 6d, e and f; Supplementary Data Tables S3), corresponding to subchondritic $\varepsilon_{Hf}(t)$ = −5.0 ± 1.8 (n = 7) for sample SR-4, −3.8 ± 1.5 (n = 7) for sample SR-19 and −4.5 ± 1.4 (n = 4) for sample SR-36 and two stage Hf model age (T_{DM2}) at ca. 2.60 Ga (Fig. 7 and Supplementary Data Table S3). Two zircon grains in sample SR-36 show significantly lower $^{176}Hf/^{177}Hf_{1.77\ Ga}$ ratios of 0.281359 ± 0.000004 (n = 2) with corresponding $\varepsilon_{Hf}(t)$ = −10.6 ± 0.1 and T_{DM2} = 2.93 ± 0.01 Ga, which may point to the involvement of a heterogenous source.

Most of the Neoarchean and early Paleoproterozoic zircon xenocrysts exhibit superchondritic $\varepsilon_{Hf}(t)$ values (2684–2703 Ma: +1.2 to +2.3; 2356–2429 Ma: +3.3 to +6.4; Table 3 and Supplementary Data Table S3). All these xenocrysts (commonly cores) show an oscillatory zoning (Fig. 5a-v, c-iii, c-iv and c-v) and high Th/U ratios of 0.33–1.12 (Supplementary Data Table S2), indicative of an igneous origin. In contrast, all late Paleoproterozoic xenocrysts reveal subchondritic $\varepsilon_{Hf}(t)$ values (1792–1828 Ma: −4.8 to −3.7) and relatively low Th/U ratios of 0.10–0.42, but also show an oscillatory zoning (Fig. 5b-iv and b-v). It is worth noting that the initial Hf isotope compositions of some ca. 1800 Ma zircon xenocrysts are nearly identical to those of the ca. 1770 Ma magmatic domains, particularly in sample SR-19 (Table 3).

4.3.2. Salumbar granitoids

Like Sarada, the Salumbar zircon grains also yield variable $^{207}Pb/^{206}Pb$ ages, ranging from 1720 Ma to 2703 Ma in sample 2NG-8 (25 spot analyses on 21 grains; Supplementary Data Table S2) and from 1252 Ma to 1786 Ma in sample 2NG-9 (25 spot analyses on 22 grains). In sample 2NG-8, most zircon grains define an upper intercept age of 1770 ± 3 Ma (MSWD = 1.1; n = 20), which is identical to the concordia age of 1767 ± 5 Ma obtained from fifteen zircon domains (Fig. 8a). In sample 2NG-9, five zircon grains yield a concordia age of 1769 ± 7 Ma (Fig. 8b). These concordia ages from both samples are interpreted to represent the time of crystallisation of the Salumbar granitoids.

A few zircon grains in sample 2NG-8 yield older concordant ages between 1800 Ma and 2703 Ma (Tables 3 and Supplementary Data Table S2), which are interpreted as xenocrysts. Moreover, a younger concordant rim at 1720 ± 15 Ma (concordance level = 104%) with very low Th/U of 0.06, surrounding an older core of 2492 ± 17 Ma (Th/U = 0.44; concordance level = 93%; Fig. 5d-iii) perhaps result from a metamorphic overprint at ca. 1720 Ma.

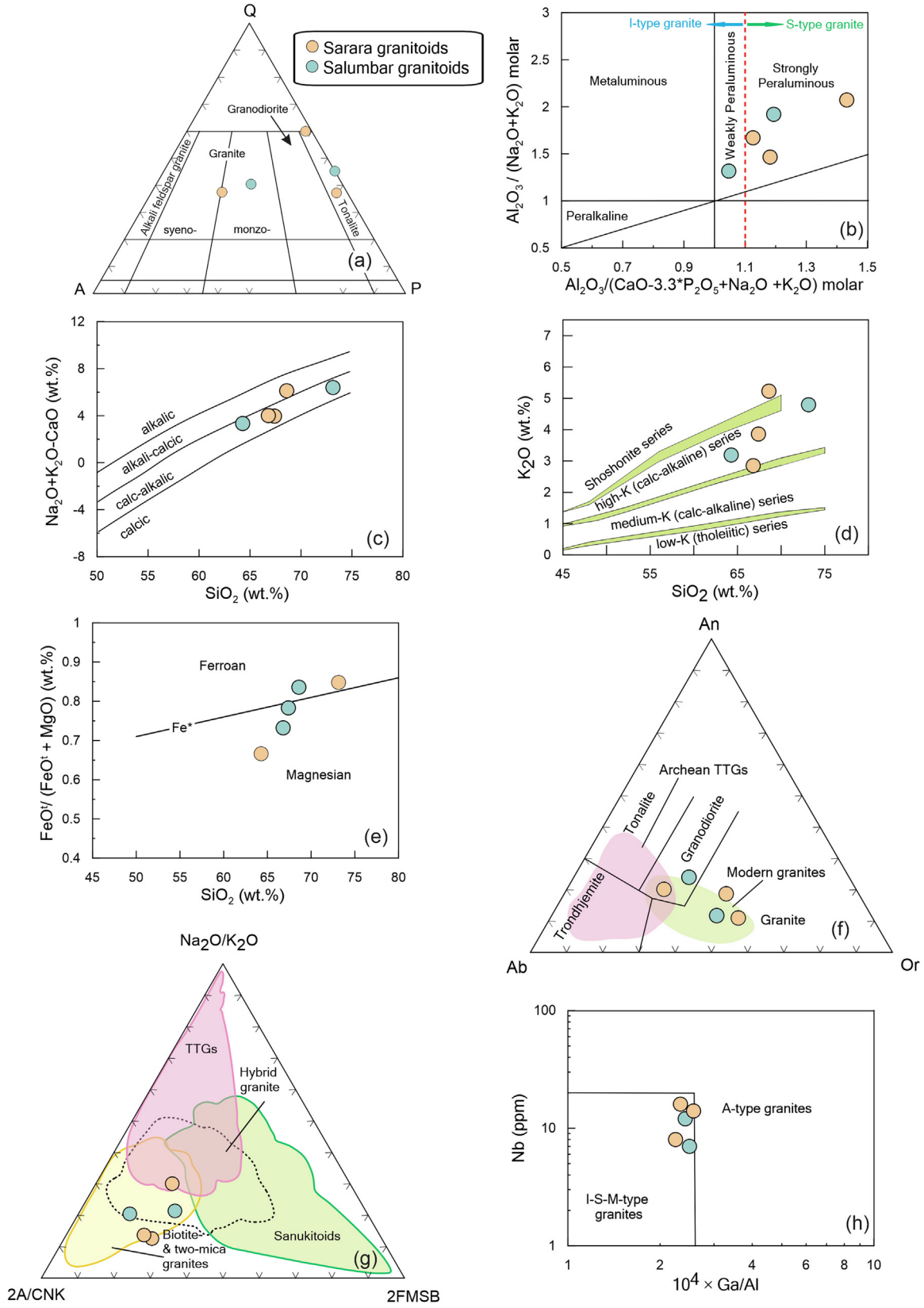

Fig. 3. Characterisation and classification of the Sarada and Salumbar granitoids. (a) Modal abundances of plagioclase (P), quartz (Q) and alkali feldspar (A) in diagram of Streckeisen (1976), (b) molar $Al_2O_3/(CaO - 3.3P_2O_5 + Na_2O + K_2O)$ versus molar $Al_2O_3/(Na_2O + K_2O)$ Shand classification diagram (Maniar and Piccoli, 1979); the division between weakly peraluminous and strongly peraluminous is from Bucholz et al. (2018) and that of I-type – S-type granites is from Chappell and White (1974), (c) modified alkali-lime index, $Na_2O + K_2O - CaO$ (wt%) versus SiO_2 (wt.%) diagram (Frost et al., 2001), (d) K_2O (wt.%) versus SiO_2 (wt.%) diagram (Rickwood, 1989), (e) $FeO^t/(FeO^t + MgO)$ versus SiO_2 plot (Frost et al., 2001) with Fe-index (Fe*) line as modified by Frost and Frost (2008), (f) CIPW normative Or-An-Ab diagram (Barker, 1979) with fields of Archean TTGs and modern granites after Moyen and Martin (2012), (g) major and trace elements 2FMSB [$(FeO^t + MgO)$ wt.% × (Sr + Ba) wt.%] – 2A/CNK[$Al_2O_3/(CaO - 3.3P_2O_5 + Na_2O + K_2O)$] –$Na_2O/K_2O$ diagram (Laurent et al., 2014) and (h) Nb (ppm) versus $10^4 \times Ga/Al$ discrimination plot (Whalen et al., 1987).

Table 2
Whole rock chemical compositions (major elements in wt.%, trace elements in ppm) for the dated samples of the southern Aravalli orogen, NW India.

Sample no.	SR-4[a]	SR-19[a]	SR-36[b]	2NG-8[a]	2NG-9[b]
SiO_2	67.4	66.8	68.6	64.3	73.1
TiO_2	0.60	0.62	0.41	0.74	0.37
Al_2O_3	16.16	15.98	14.59	16.42	13.63
$Fe_2O_3^t$	5.22	4.59	4.19	5.88	2.42
MnO	0.10	0.05	0.14	0.05	0.03
MgO	1.30	1.51	0.74	2.65	0.39
CaO	2.10	2.78	1.72	2.96	1.54
Na_2O	2.20	3.94	2.61	3.10	3.14
K_2O	3.86	2.85	5.23	3.19	4.80
P_2O_5	0.14	0.18	0.31	0.07	0.05
LOI	1.19	1.16	1.81	1.07	0.91
Sum	100.3	100.5	100.3	100.4	100.4
V	51	47	24	73	24
Cr	40	40	<20	120	<20
Ni	<20	<20	<20	20	<20
Zn	80	40	60	50	<30
Ga	22	19	18	21	18
Rb	187	138	211	216	196
Sr	140	184	141	233	115
Y	19	13	43	14	13
Zr	220	222	288	218	342
Nb	14	8	16	12	7
Ba	772	673	724	513	766
Pb	14	22	34	12	27
Th	27.3	24.2	18.2	27.3	55.4
U	4.1	2.8	4.2	2.8	5
Hf	5.5	4.8	6.8	4.9	7.6
Ta	1.4	0.6	2.4	1.3	0.8
La	63.8	66.4	48.9	65.4	157
Ce	124	119	94.9	124	269
Pr	13.9	13.0	10.8	13.1	25.2
Nd	50.7	45.9	39.8	46.8	77.6
Sm	9.6	7.1	7.5	7.9	9.3
Eu	1.43	1.31	1.36	1.51	0.88
Gd	6.1	4.0	6.5	4.8	5.0
Tb	0.8	0.5	1.2	0.6	0.6
Dy	4.2	2.7	7.8	3.0	2.9
Ho	0.7	0.5	1.6	0.5	0.5
Er	1.9	1.3	5.0	1.2	1.2
Tm	0.27	0.17	0.78	0.14	0.17
Yb	1.8	1.1	5.4	0.9	1.1
Lu	0.28	0.16	0.83	0.13	0.17
∑REE	279.5	263.1	232.4	270.0	550.6
$(La/Yb)_N$	25.3	43.2	6.5	51.9	102.0
$(Gd/Yb)_N$	2.8	3.0	1.0	4.3	3.7
Eu/Eu*	0.57	0.74	0.59	0.74	0.39
ASI	1.43	1.13	1.18	1.19	1.05
CaO/Na_2O	0.95	0.71	0.66	0.95	0.49
Al_2O_3/TiO_2	26.9	25.8	35.6	22.2	36.8
Zrn T (°C)	837	811	842	813	857

Note: a = Tonalite, b = Granite.
N: Chondrite normalised. $Eu/Eu^* = Eu_N/(Sm_N \times Gd_N)^{½}$.
ASI: Aluminium Saturation Index = molar $Al_2O_3/(CaO\text{-}3.3P_2O_5 + Na_2O + K_2O)$.
Zrn T (°C): Zircon saturation temperature.

The initial Hf isotope compositions of the zircon grains in the Salumbar granitoids are variable. Sample 2NG-8 yields $^{176}Hf/^{177}Hf_{1.77\ Ga}$ ratio of 0.281540 ± 0.000041 (n = 8), corresponding to subchondritic $\varepsilon_{Hf}(t)$ = –4.2 ± 1.5 and T_{DM2} = 2.59 ± 0.08 Ga (Figs. 7 and 8c; Tables 3 and Supplementary Data Table S3). In contrast, sample 2NG-9 shows significantly lower $^{176}Hf/^{177}Hf_{1.77\ Ga}$ ratio of 0.281365 ± 0.000029 (n = 10), which correspond to subchondritic $\varepsilon_{Hf}(t)$ = –10.3 ± 1.0 and T_{DM2} = 2.92 ± 0.05 Ga. Notably, the Hf isotope compositions of this sample overlap with those obtained from some zircon grains in sample SR-36 of the Sarada granitoids (Table 3). Zircon domains with younger $^{207}Pb/^{206}Pb$ ages (1252–1703 Ma; n = 19) in sample 2NG-9, showing similar initial $^{176}Hf/^{177}Hf_{1.77\ Ga}$ ratios like the older (ca. 1770 Ma) domains, suggest (perhaps multiple) post-zircon growth Pb-loss (Fig. 8d).

The oldest xenocryst, dated at 2703 ± 20 Ma (Fig. 5d-v; Th/U = 0.30; concordance level = 100%), shows the lowest $^{176}Hf/^{177}Hf_{2.70\ Ga}$ ratio of 0.281078, corresponding to superchondritic $\varepsilon_{Hf}(t)$ = +1.2 and T_{DM2} = 3.05 Ga (Fig. 8c). A late Paleoproterozoic structureless xenocryst with low Th/U = 0.06 was dated at 1840 ± 25 Ma (Fig. 5d-iv; concordance level = 96%). This grain, which has an initial $^{176}Hf/^{177}Hf_{1.84\ Ga}$ = 0.281519 ($\varepsilon_{Hf}(t)$ = – 3.3 ± 0.8 and T_{DM2} = 2.60 Ga), most likely formed during a metamorphic event prior to granitoid emplacement.

Table 3
Summary of U-Pb and Lu-Hf isotope data from the Sarada and Salumbar granitoids, southern Aravalli orogen, NW India.

Locality/ Sample no.	Age ± 2σ (Ma)[a]		c/s/z[b]	$^{176}Hf/^{177}Hf_{int}$[c] (Mean)	±2σ (×10^{-5})	εHf_{int}[d] (Mean)	±2σ	No.[e]	Interpretation
Sarada[f]									
SR-4	1759 ± 7	u.i.	18/25/23						
	1762 ± 6	conco.	13/25/23	0.281521	5	−5.0	1.8	07/10	Magmatic event
	2429 ± 30	conc.	01/25/23	0.281405	3	+6.4	1.1	01/10	Inherited
	1828–1792	conc. to disc.	02/25/23	0.281507	2	−4.8	0.8	01/10	Inherited
	1734 ± 13	conc.	01/25/23	0.281267	2	−14.6	0.7	01/10	Metamorphic event
	1703–1749	conc.	04/25/23						Metamorphic event
SR-19	1768 ± 8	u.i.	13/25/24						
	1770 ± 8	conco.	10/25/24	0.281550	4	−3.8	1.5	07/10	Magmatic event
	1797 ± 8	conco.	04/25/24	0.281533	3	−3.7	1.2	03/10	Inherited
	1582–1699	conc. to disc.	06/25/24						Pb-loss
SR-36	1767 ± 5	u.i.	18/25/23						
	1768 ± 6	conco.	13/25/23	0.281532	4	−4.5	1.4	04/10	Magmatic event
				0.281359	1	−10.6	0.1	02/10	
	2684 ± 15	conc.	01/25/23	0.281124	2	+2.3	0.8	01/10	Inherited
	2420 ± 17	conc.	01/25/23	0.281326	3	+3.3	0.9	01/10	Inherited
	2356 ± 19	conc.	01/25/23	0.281392	3	+4.2	1.1	01/10	Inherited
	2356 ± 18	conc.	01/25/23	0.281124	2	−5.3	0.7	01/10	Inherited
	2521–2673	conc. to disc.	03/25/23						Inherited
Salumbar									
2NG-8	1770 ± 3	u.i.	20/25/21						
	1767 ± 5	conco.	15/25/21	0.281540	4	−4.2	1.5	08/10	Magmatic event
	2703 ± 20	conc.	01/25/21	0.281078	2	+1.2	0.7	01/10	Inherited
	1840 ± 25	conc.	01/25/21	0.281519	2	−3.3	0.8	01/10	Inherited/Meta
	2492 ± 17	disc.	01/25/21						Inherited
	1799 ± 13	conc.	01/25/21						Inherited
	1720 ± 15	conc.	01/25/21						Metamorphic event
2NG-9	1769 ± 7	conco.	05/25/22	0.281365	3	−10.3	1.0	10/10	Magmatic event
	1252–1703	conc. to disc.	19/25/22						Pb-loss

Note: Meta = metamorphic zircon.
[a] Intrusion age; u.i.: upper intercept age; conco.: concordia age; conc.: concordant age; disc.: discordant age.
[b] c/s/z; c: number of zircon analyses used for age calculation; s: number of spot analyses per sample; z: number of zircon grains analysed per sample.
[c] average $^{176}Hf/^{177}Hf_{int}$ calculated by using the ages given in column 2.
[d] average εHf_{int} calculated by using the ages given in column 2.
[e] number of zircon spots used for mean $^{176}Hf/^{177}Hf_{int}$ and εHf_{int} calculation/Lu-Hf spot analyses per sample.
[f] for location coordinates, see Table 1.

5. Discussion

5.1. Timing and nature of magmatism

In this study, late Paleoproterozoic S-type granites dated at 1770–1760 Ma are reported for the first time from the Aravalli orogen, particularly from its southern domain. This region has traditionally been regarded as an exclusively Archean terrane, as post-Archean igneous rocks have not been reported to date. Presently, evidence for a ca. 1770 Ma magmatic event is limited to a small number of zircon xenocrysts found in an A-type granite (ca. 1730 Ma) from the northern Aravalli orogen (Kaur et al., 2017c), and to the detrital zircon record across the Aravalli orogen. These zircon xenocrysts suggest the existence of an unexposed ca. 1770 Ma crustal substrate in the northern part of the orogen. Pronounced detrital zircon age peaks between 1770 Ma and 1760 Ma across the Aravalli orogen (Fig. 7), along with deposition of ca. 1750 Ma clastic sedimentary rocks in collision-related basins of the northern part of the orogen, suggest that a substantial volume of ca. 1770 Ma magmatic rocks must have been exposed and subsequently eroded away. The remnants of this crust are now likely concealed beneath younger rocks.

The geochronological data obtained during the present and previous studies suggest a three-stage magmatic evolution in the Aravalli orogen during late Paleoproterozoic. The earliest stage is represented by granitoids and felsic volcanic rocks emplaced at 1875–1810 Ma in a continental-arc setting. The second stage, dated at 1770–1760 Ma, is marked by the intrusion of S-type granites in a *syn*-collisional setting. The third stage at 1730–1700 Ma, involved the emplacement of A-type granites and charnockites in a post-collisional extension-related tectonic regime. This final stage has been linked to slab break-off, marking the termination of a protracted period of subduction that began at ca. 1875 Ma (Kaur et al., 2017a, 2023a). The emplacement of the Sarada-Salumbar S-type granitoids at 1770–1760 Ma perhaps related to the collision of microterranes with the previously formed continental magmatic arc. This collisional setting is supported by the geochemical characteristics of the granitoids, particularly their Rb, Y, Nb, Ta and Yb abundances (Fig. 9).

Evidence of a pre-collisional metamorphic overprint in the southern part of the Aravalli orogen is provided by a zircon xenocryst with Th/U < 0.1, which yielded an age of ca. 1840 Ma. Post-collisional metamorphism is suggested by zircon overgrowths with ages of ca. 1720 Ma, surrounding older magmatic cores. The last

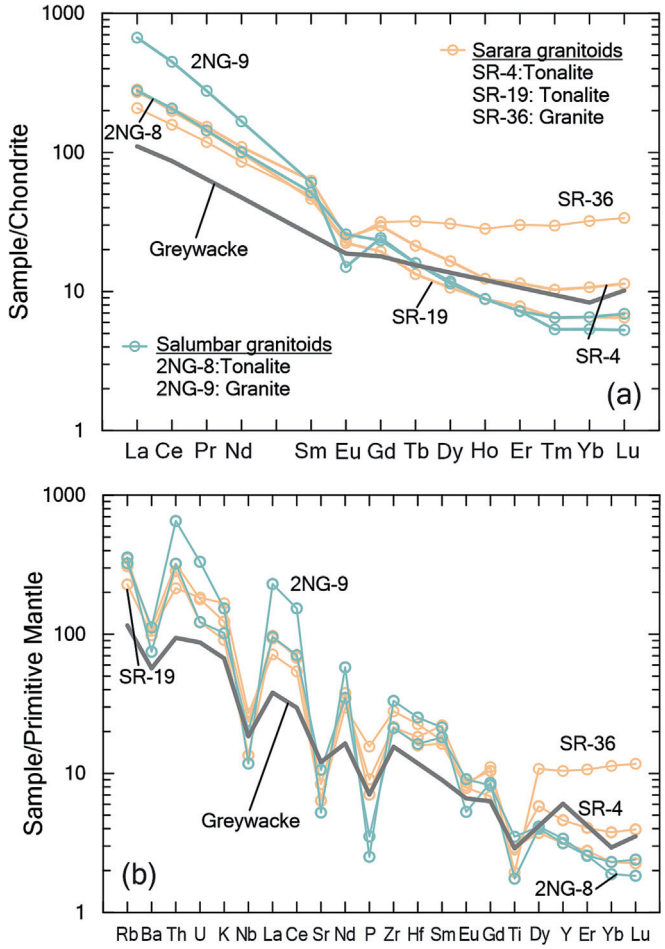

Fig. 4. (a) Chondrite-normalised REE and (b) primitive mantle-normalised multi-element diagrams for the Sarada and Salumbar granitoids. Chondrite-normalising values are after Barrat et al. (2012) and those of primitive mantle are after Palme and O'Neill (2014). Late Archean greywacke: Condie (1993).

event is very likely related to the emplacement of A-type granites at ca. 1720 Ma, although such rocks have not yet been reported from the southern Aravalli orogen.

5.2. Source characteristics and magma genesis

S-type granites are commonly thought to be the result of anatexis of metasedimentary rocks, such as *meta*-greywackes or metapelites or both in the middle-lower crust (Chappell and White, 1974, 2001; Patiño Douce and Beard, 1995; Stevens et al., 2007; Bucholz and Spencer, 2019; Nabelek, 2020). The high CaO/Na_2O ratios (> 0.3; Table 2) suggest that the Sarada-Salumbar granitoids were predominantly formed by partial melting of *meta*-greywackes (Fig. 10a). This interpretation is also supported by their relatively low Rb/Sr ratios (0.8–1.7; Fig. 10b). The studied granitoids yield high zircon saturation temperatures (811–857 °C) (Watson and Harrison, 1983), which indicate the upper-temperature estimate of melting due to significant inheritance of zircon grains in these granitoids (Miller et al., 2003). In addition, the Al_2O_3/TiO_2 ratio, which is a function of melting temperature (Jung and Pfänder, 2007; Bucholz and Spencer, 2019), is quite low (<100; Table 2) in the investigated granitoids, pointing partial melting at high temperatures. This is due to the retention of Al_2O_3 in the refractory aluminous phase and increase in liberation of TiO_2 with the breakdown of Ti-bearing phases (such as biotite and ilmenite) with rising temperature (Sylvester, 1998). Therefore, the high zircon saturation temperatures and low Al_2O_3/TiO_2 ratios of the studied granitoids are both indicative for high melting temperature (>800 °C) during magma genesis.

Partial melting of a heterogeneous sequence of sedimentary rocks is further reflected by significant variation in zircon Hf isotope compositions within the studied granitoids (Sarada: ε_{Hf}(1.77 Ga) = −10.6 to −2.8; Salumbar: ε_{Hf}(1.77 Ga) = −11.0 to −2.6). We note that zircon grains in sample SR-36 of the Sarada granite show ε_{Hf}(1.77 Ga) variation of nearly 7 epsilon units (−10.6 to −3.1). Such wide variations indicate that these granitoids were derived from different melt batches that formed within a heterogeneous crust and were incompletely mixed with each other. Alternatively, such a variation in Hf isotopes could be due to disequilibrium melting of zircon at source, which resulted in the generation of isotopically distinct batches of melts (Tang et al., 2014). Although melt input from mantle cannot be ruled out, the predominance of highly subchondritic $\varepsilon_{Hf}(t)$ values suggest a major contribution from crustal melts. This is further supported by high $(La/Sm)_N$ ratios (4.26–10.99), and low Nb/La (0.04–0.33) and Nb/Ce (0.03–0.17) ratios of the granitoids compared to average mantle values (Khaksar et al., 2022 and references therein), and the enrichment of LILE and LREE in mantle-normalised multielement patterns (Fig. 4b).

Hafnium model ages of 2.95–2.52 Ga point to reworking of Meso- to Neoarchean crust, which is also supported by the presence of inherited zircon grains with ages of 2500–2700 Ma. Additionally, inherited zircon grains with ages of 2356–2429 Ma and 1792–1800 Ma provide direct evidence for the involvement of detritus derived from Paleoproterozoic crust during formation of the S-type granites. The detrital zircon ages of 2500–2550 and ca. 1800 Ma correspond to the Neoarchean TTG-sanukitoid-potassic granites and continental–arc magmatic rocks in the Aravalli orogen, respectively (Kaur et al., 2017a, 2017c, 2019b, 2021, 2023a). However, no outcrops of early Paleoproterozoic ages (2356–2429 Ma) have been reported to date from the Aravalli orogen or its hinterland. Although 2378–2432 Ma granitoids (Ahmad et al., 2009) have been reported from the Bastar Craton in eastern India (Fig. 1a) and may represent possible sources for these inherited zircon grains, no zircon Hf isotope data from these granitoids are available to confirm this. Moreover, the initial Hf isotope compositions of the inherited zircon grains indicate a superchondritic nature of the Neoarchean crust ($\varepsilon_{Hf}(t)$ = +1.2 to +2.3; Fig. 7) and compositionally variable early Paleoproterozoic crust ($\varepsilon_{Hf}(t)$ = −5.3 to +3.3). Therefore, the combined dataset provides strong evidence for the involvement of distinct Neoarchean and Paleoproterozoic crustal components in the genesis of the Aravalli S-type granites at 1770–1760 Ma.

5.3. Geodynamic implications

The central and northern Aravalli orogen record the emplacement of continental-arc granitoids at ca. 1875 Ma and 1850–1810 Ma, respectively. This indicates that the subduction continued for at least 65 Myr from 1875 Ma to 1810 Ma (Kaur et al., 2023a). The emplacement of ca. 1810 Ma continental-arc granitoids may mark the stage of initial collision between the continental crust of west and east Aravalli terranes (Fig. 11a), during which subduction of oceanic lithosphere was still ongoing (cf. Zhu et al., 2015).

The depositional age of the siliciclastic sediments (quartzite) intruded by the ca. 1850 Ma continental-arc granitoids in the northern Aravalli orogen is constrained at ca. 1854 Ma, which not only overlaps with the timing of continental-arc magmatism but also coincides with the age of high-grade regional metamorphism (Kaur et al., 2013a; Ozha et al., 2016). Such temporal overlap indicates a highly active geodynamic regime in the Aravalli orogen at this time, when magmatism, sedimentation and metamorphism

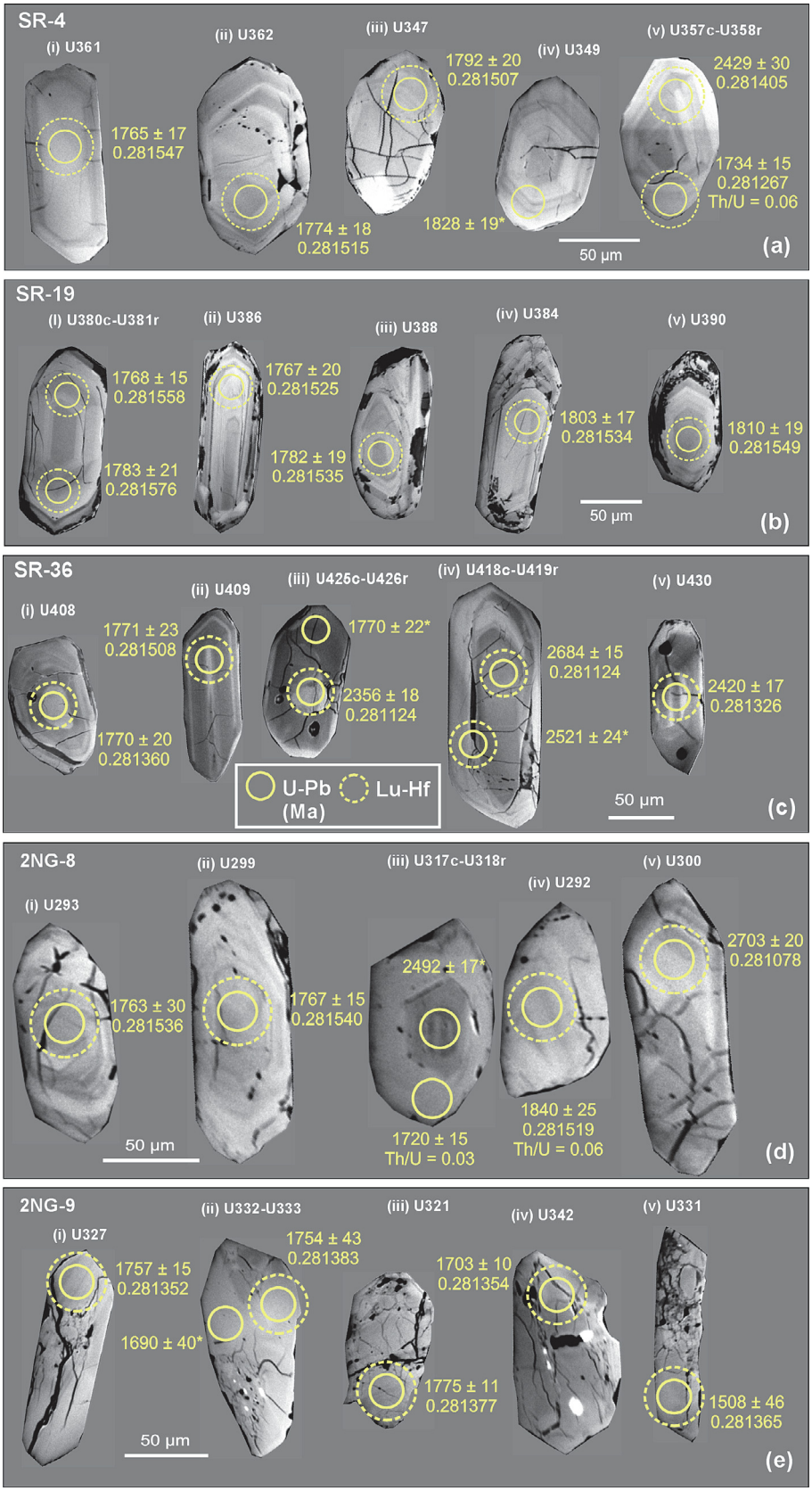

Fig. 5. Representative back-scattered electron images of the Sarada (a, b and c), and Salumbar (d and e) zircon grains, showing laser spot positions and results of U-Pb dating (Ma) and Hf-isotope compositions. Most of ages are concordant $^{207}Pb/^{206}Pb$ ages (concordance level: 95% –105%) and * indicates discordant ages.

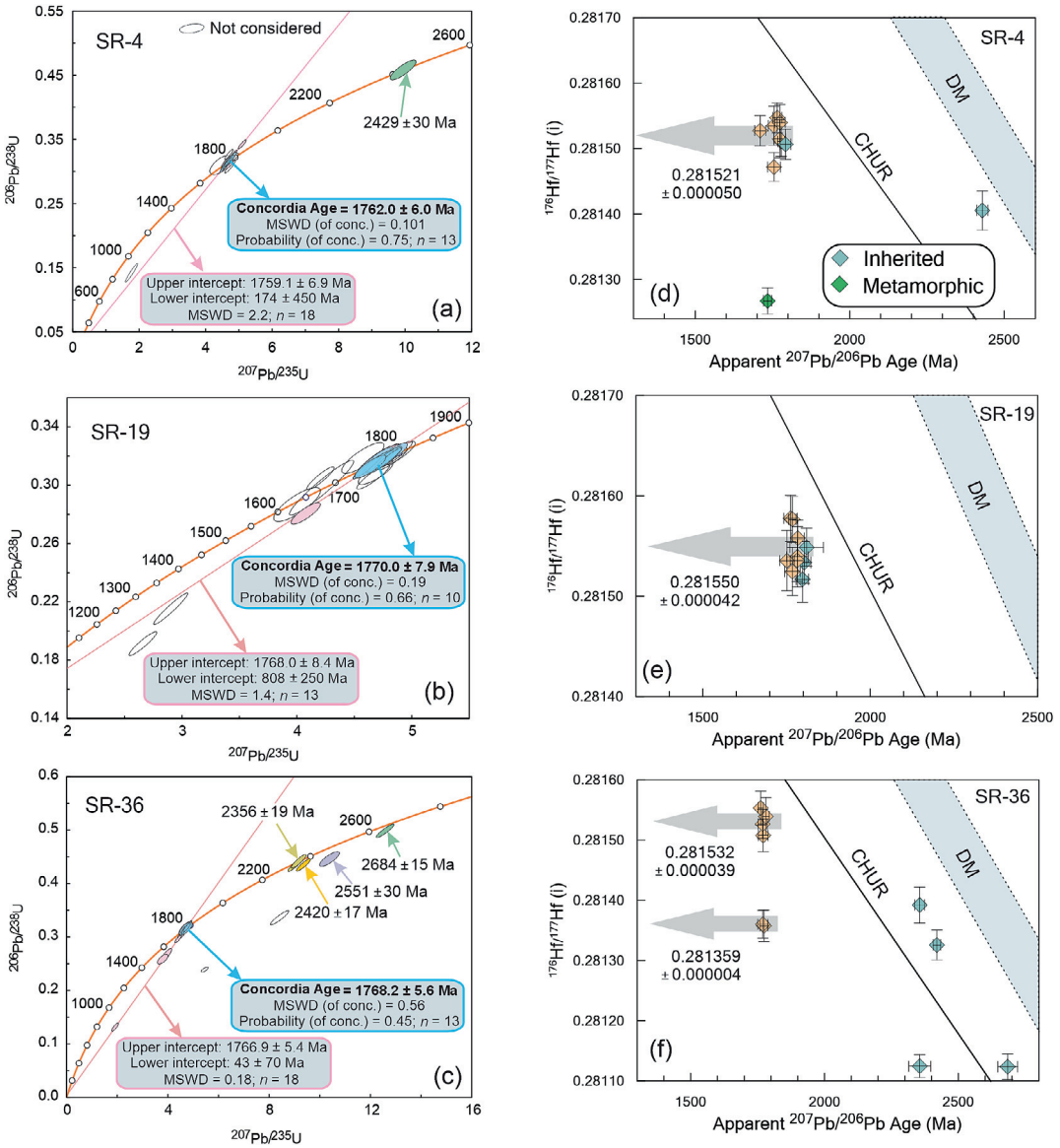

Fig. 6. (a, b and c) Concordia diagrams and (d, e and f) $^{207}Pb/^{206}Pb$ age versus initial $^{176}Hf/^{177}Hf$ ratios showing the results of zircon U-Pb dating and Lu-Hf isotope composition, respectively for the Sarada granitoids. CHUR = Chondritic uniform reservoir and DM = depleted mantle.

were apparently synchronous (for details, see Kaur et al., 2013a, 2017a), consistent with the compressional tectonics in a subduction-accretion environment (Abati et al., 2010).

The compressional regime appears to have been maintained until 1770–1760 Ma during which the S-type granites were formed by partial melting of metasedimentary rocks within the overriding plate at mid- to lower-crustal depths. At this stage the microterrane was dragged downward by the subducting oceanic slab, causing compressional tectonics in the lower to middle crust (Fig. 11b). The heat required for the melting of the metasedimentary source rocks may be acquired by deep burial, radioactive decay or the ponding basaltic magmas beneath the low-density sediments (Eriksson et al., 1995; Sylvester, 1998; Zhu et al., 2020).

Given the considerably large volume of the S-type granites, we propose that these likely were produced by enhanced mantle wedge flow, induced by slab roll-back (Fig. 11b) and high angle subduction as a consequence of terrane collision (Magni et al., 2012). Such enhanced mantle wedge flow would have promoted large-scale melting of metasedimentary rocks in the overlying crust.

Evidence for a Paleoproterozoic suture zone in the central and southern Aravalli orogen is marked by fault-bounded, sheared and brecciated mantle-wedge-related antigorite serpentinites, considered as remnants of an ophiolite suite exhumed along a curvilinear Rakhabdev Shear Zone (Sen, 1981; Chattopadhyay and Gangopadhyay, 1984; Bakliwal and Ramasamy, 1987; Sinha-Roy, 1988; Sarkar et al., 2020). This shear zone, traceable for at least 140 km (Fig. 1b; Bakliwal and Ramasamy, 1987), has been interpreted as a paleo-subduction zone along which these hydrated mantle rocks were exhumed during ongoing subduction, culminating in a crustal-scale collisional boundary (Sarkar et al., 2020). The exhumation of these rocks along the subduction channel most likely occurred during 1875–1810 Ma, preceding the emplacement of the S-type granites. Furthermore, there is evidence for the juxtaposition of two distinct litho-successions with contrasting geomorphology and depositional settings across the shear zone (Bhattacharya and Mukherjee, 2020). These authors suggested that the western succession (continental to shallow marine) was unconformably deposited on the gneissic basement, whereas the eastern succession (deep-water turbidites) was

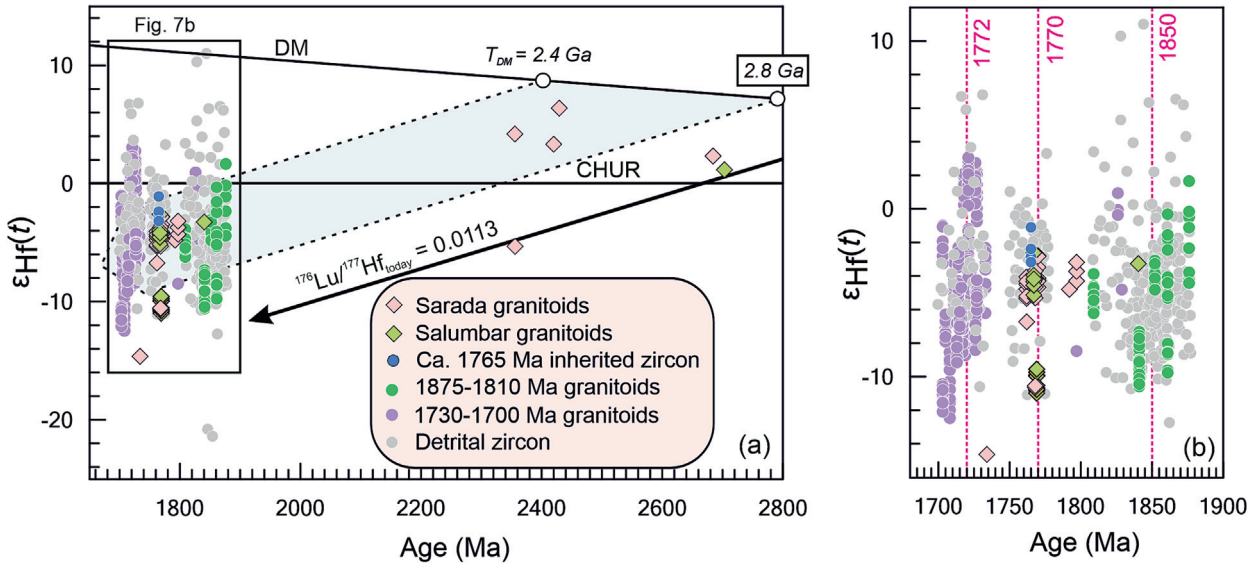

Fig. 7. (a and b) Zircon age versus $\varepsilon_{Hf}(t)$ diagram showing data of the Sarada and Salumbar granitoids in comparison with relevant published igneous and detrital zircon data from the Aravalli orogen. Data source: ca. 1765 Ma inherited zircon – Kaur et al. (2017c); 1875 1810 Ma Aravalli continental arc granitoids – Kaur et al. (2017a, 2023a); 1730–1700 Ma A-type granites – Kaur et al. (2017c, 2021, 2025), Detrital zircon – Kaur et al. (2011a, 2013a, 2019a, 2022, 2023a, 2023b) and Wang et al. (2017, 2019); CHUR = Chondritic uniform reservoir and DM = depleted mantle. $^{176}Lu/^{177}Hf_{today}$ = 0.0113: evolution of average continental crust (Taylor and McLennan, 1985; Wedepohl, 1995).

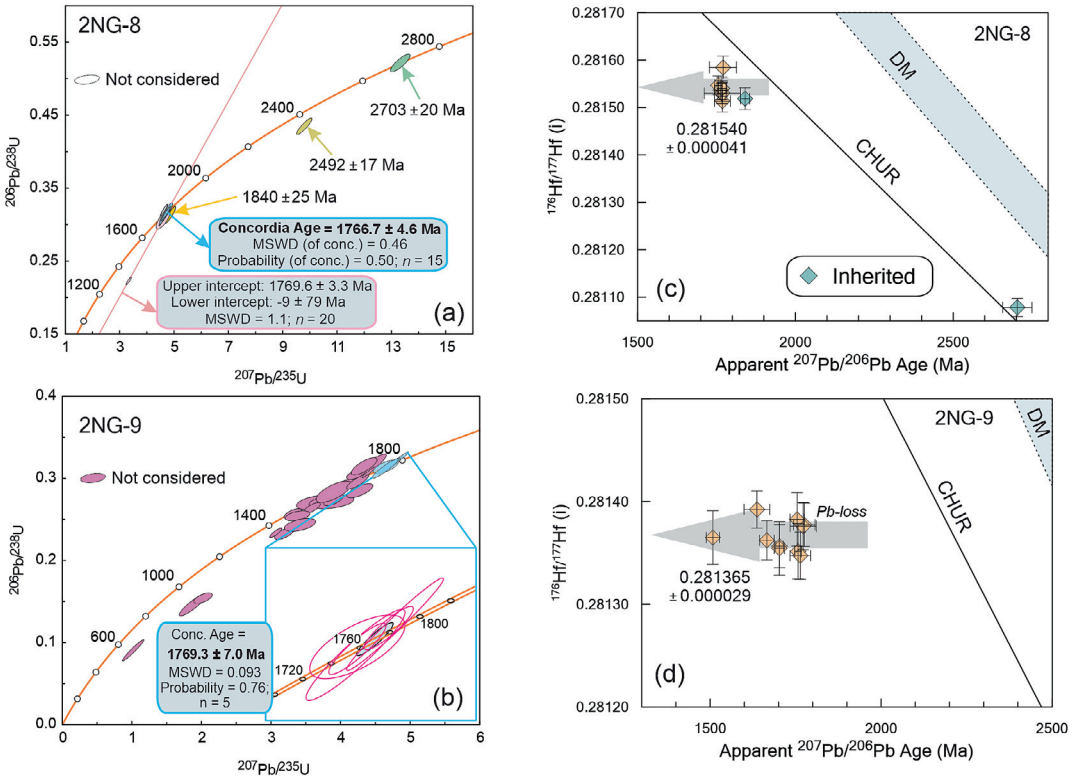

Fig. 8. (a and b) Concordia diagrams and (c and d) $^{207}Pb/^{206}Pb$ age versus initial $^{176}Hf/^{177}Hf$ ratios showing the results of zircon U-Pb dating and Lu-Hf isotope composition, respectively for the Salumbar granitoids. CHUR = Chondritic uniform reservoir and DM = depleted mantle.

deposited on a relatively old sedimentary succession. It is noteworthy that the studied S-type granitoids occur east of the Rakhabdev Shear Zone, further supporting an eastward polarity of subduction. Furthermore, the occurrence of 1730–1700 Ma A-type granites in the northern and central parts of the Aravalli orogen provides substantial evidence for widespread post-collisional extensional magmatism. This magmatic activity occurred over a relatively short duration of ca. 30 Myr and terminated abruptly at ca. 1700 Ma. We note that the A-type magmatism was locally accompanied by within-plate mafic magmatism in the northern domain, and granulite metamorphism and charnockite magmatism in the central domain of the Aravalli orogen, suggesting a high-temperature regime in the lower/middle crust and magma input from the mantle (Kaur et al., 2013b, 2017c, 2021, 2025).

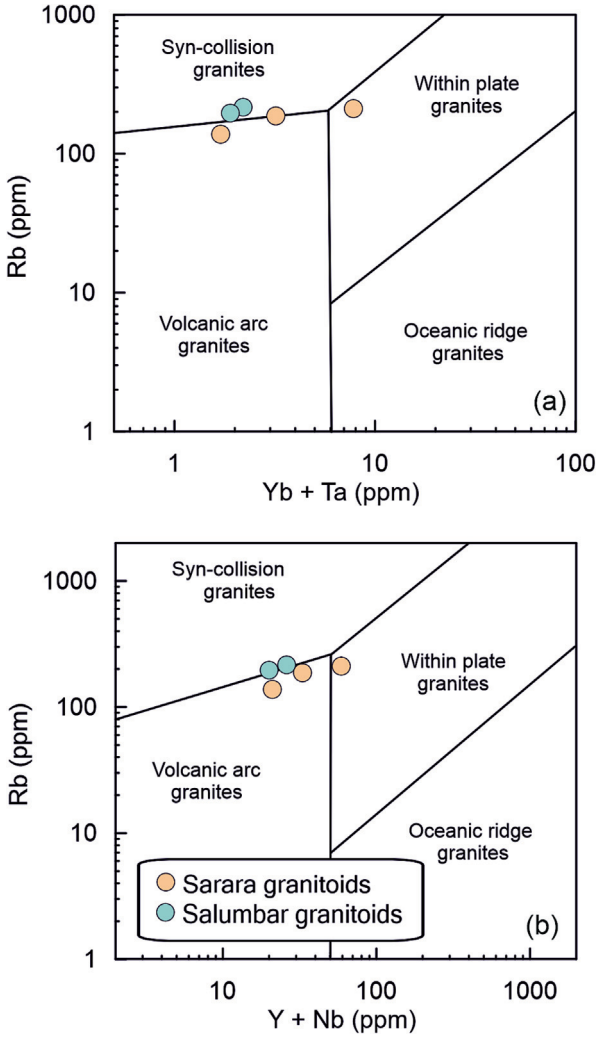

Fig. 9. Tectonic discrimination diagrams (a) Rb (ppm) versus Yb + Ta (ppm) and (b) Rb (ppm) versus Y + Nb (ppm) (Pearce et al., 1984) for the Sarada and Salumbar granitoids.

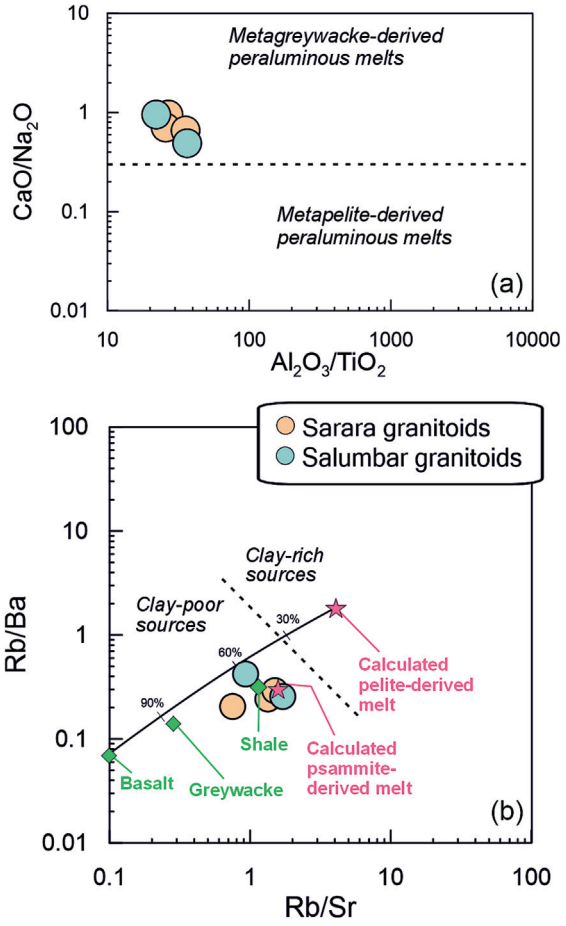

Fig. 10. Source discrimination diagrams (a) Al_2O_3/TiO_2 versus CaO/Na_2O and (b) Rb/Sr versus Rb/Ba (Sylvester, 1998).

It is suggested that the transition from a compressional to an extensional tectonic regime occurred at ca. 1720 Ma due to buoyancy of the lower continental plate, which reduced the slab pull force and ultimately led to slab break-off and cessation of subduction following collision (Zhu et al., 2015). Slab break-off likely opened a slab window that triggered partial melting of the crust due to a temperature increase of the lithosphere, but also limited melting of the underlying mantle owing to inflow of hot asthenosphere and uplift related pressure reduction (Zhu et al., 2015). This resulted in granulite-facies metamorphism, as well as the widespread formation and intrusion of A-type granites and coeval charnockites (Fig. 11c; for details, see Kaur et al., 2025).

5.4. Regional and global comparisons

Paleoproterozoic S-type granites are rarely reported from the Indian cratons and their adjoining mobile belts. A possible occurrence of ca. 1600 Ma S-type granites has been documented around Beawar in the west-central Aravalli orogen (Fig. 1b) by Kaur et al. (2020), which are characterised by highly subchondritic $\varepsilon_{Hf}(t)$ values and Neoarchean two-stage Hf model ages (Table 4). The S-type granites reported from the Chotanagpur Gneissic Complex (ca. 1565 Ma; Qasim et al., 2025), eastern India (Fig. 1a) and the Garhwal Himalaya (ca. 1845 Ma; Mishra et al., 2019, 2022), northwest India show subchondritic $\varepsilon_{Nd}(t)$ values and Archean to early Paleoproterozoic model ages.

Globally, Paleoproterozoic S-type granites have been reported mainly from China, including 2350–2430 Ma and 1840–1950 Ma from the Khondalite Belt, North China Craton (Yin et al., 2011; Zhang et al., 2017; Li et al., 2022; Shi et al., 2022), 1930 2040 Ma from the Yangtze Block, South China Craton (Wang and Dong, 2019; Li et al., 2021) and 1840–1878 Ma from the Cathaysia Block, South China Craton (Xia et al., 2012; Chen and Xing, 2013). Additional minor occurrences of Paleoproterozoic S-type granites are documented from the Siberian Craton (ca. 1900 Ma; Turkina et al., 2006), Ukrainian Shield (2050 2070 Ma; Savko et al., 2014) and Guyana Shield (ca. 1960 Ma; Almeida et al., 2007). These granites are predominantly characterised by subchondritic $\varepsilon_{Hf}(t)$ and/or $\varepsilon_{Nd}(t)$ values and Archean Hf-Nd model ages (Table 4). Collectively, the available data indicate that Paleoproterozoic S-type magmas were predominantly generated by partial melting of Archean crustal sources. Nevertheless, exceptions include the Cathaysia Block in South China Craton and Khondalite Belt in the North China Craton where S-type magmas show varying contributions from juvenile crustal materials (Xia et al., 2012; Shi et al., 2022).

5.5. Implications for assembly of the Columbia supercontinent in NW India

A supercontinent cycle comprises three phases: subduction, collision and breakup, and occurs episodically in Earth's history, resulting in the formation of several supercontinents (Nance et al., 1988, 2014; Rogers and Santosh, 2004; Cawood et al.,

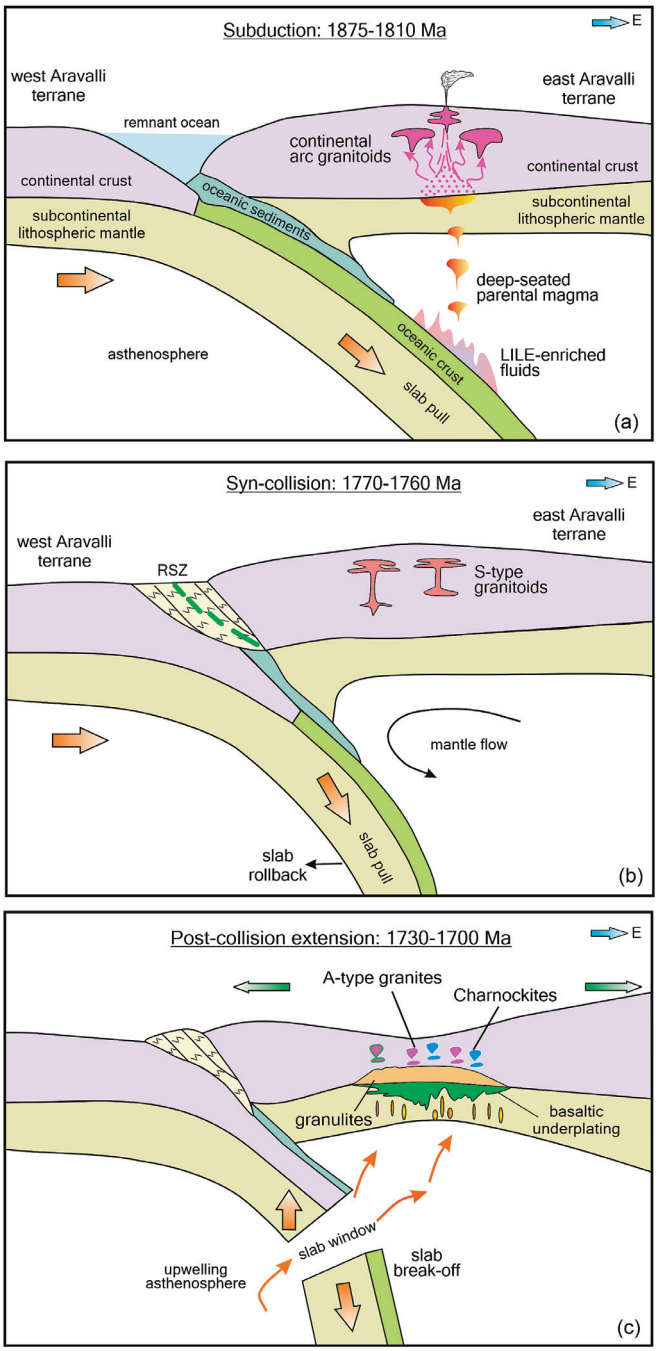

Fig. 11. Schematic model showing a sequential late Paleoproterozoic tectonic evolution of the Aravalli orogen: (a) eastward subduction of oceanic lithosphere beneath the Aravalli continental crust led to the emplacement of 1875–1810 Ma granitoids, and ca. 1810 Ma may mark the stage of initial collision between the continental crust of active and passive margins, (b) collision at ca. 1770 Ma between the west Aravalli and east Aravalli terranes, leading to formation of strongly peraluminous S-type granites and (c) slab break-off and cessation of subduction following collision opened a slab window, causing crustal uplift and extension accompanied by the upwelling of hot asthenospheric mantle into the slab window. The resultant mafic magmas accumulated at the crust-mantle boundary caused partial melting and granulitisation, resulting 1730 1700 Ma A-type granites and charnockites (after Kaur et al., 2025). RSZ: Rakhabdev Shear Zone.

2013). Columbia is considered the first coherent supercontinent, reaching its maximum packing between 1900 Ma and 1850 Ma. It either broke up at 1300–1200 Ma or underwent only modest paleogeographic changes until ca. 1000 Ma, after which it reformed as the Rodinia supercontinent (e.g., Rogers and Santosh, 2002, 2009; Zhao et al., 2002, 2004; Hou et al., 2008; Bradley, 2011; Evans and Mitchell, 2011; Johansson et al., 2022).

Although northwestern India, including Aravalli and Himalayan orogens, is known to has been involved in the assembly and breakup of the Columbia supercontinent (Kaur et al., 2009, 2013a; Bhowmik et al., 2010; Kohn et al., 2010; Mandal et al., 2016; Ozha et al., 2016; Iaccheri and Bagas, 2020; Phukon, 2022), there is no evidence that the northwest margin of proto-India formed a collisional zone during the maximum packing (1900–1850 Ma) of Columbia (Kaur et al., 2013a). Instead, the northern margin of proto-India formed part of an Andean-type continental arc system during this period, which extended from North America through Madagascar–India–Cathaysia towards East Antarctica or Central Australia (for details, see Kaur et al., 2013a). This is, for example, in contrast to the North China Craton, which preserves evidence of 2000–1850 Ma collisional event manifested as the Trans-North China Orogen (Zhao et al., 2005; Kusky and Santosh, 2009; Zhao et al., 2011; Zhao and Cawood, 2012).

From above, it can be concluded that northwestern India preserves a partial record of the Columbia supercontinent cycle. Specifically, the region shows widespread evidence of a subduction event at 1900–1850 Ma, but limited evidence for the breakup phase around 1300 Ma. Additionally, there is indication of a probable attempted breakup phase at ca. 1720 Ma (Kaur et al., 2011b). Notably, the northern Indian margin lacks evidence of collisional tectonics during the Columbia cycle, although cryptic signatures of such a phase were inferred at 1770–1750 Ma (see above). However, the discovery of ca. 1770 Ma strongly peraluminous S-type granites with a collisional signature (this study) suggests that the final stitching of the northwestern margin of India with other Columbia fragments occurred at ca. 1770 Ma, implying that the docking of northern India to the Columbia supercontinent postdated its time of maximum packing.

6. Conclusions

(1) The granitoids of Sarada and Salumbar, exposed in the southern Aravalli orogen, range in composition from granite to tonalite. They are strongly peraluminous S-type granites, showing high-K calc-alkaline, magnesian to ferroan affinities, and a *syn*-collisional tectonic setting. Their REE patterns are fractionated, characterised by depleted HREE profiles and moderate to weak negative Eu anomalies.

(2) Uranium-Pb zircon isotopic data indicate that the Sarada and Salumbar granitoids were emplaced at 1770 Ma to 1760 Ma.

(3) High CaO/Na_2O (> 0.3) and low Rb/Sr (0.8–1.7) ratios indicate that the granitoids were derived by partial melting of a *meta*-greywacke source. High zircon saturation temperatures (811–857 °C) and low Al_2O_3/TiO_2 ratios (<100) further suggest high-temperature melting conditions.

(4) The heterogeneous crustal source is indicated by subchondritic $\varepsilon_{Hf}(t)$ values, which show wide variations within individual intrusions (Sarada: $\varepsilon_{Hf}(1.77\ Ga)$ = –10.6 to –2.8 and Salumbar: $\varepsilon_{Hf}(1.77\ Ga)$ = –11.0 to –2.6).

(5) Previous and new geochronological data suggest a sequential late Paleoproterozoic crustal evolution, probably beginning with 1875–1810 Ma continental-arc magmatism, followed by ca. 1770 Ma *syn*-collisional S-type granite emplacement, and culminating in post-collisional, extension-related A-type and charnockite magmatism ca. 1720 Ma.

(6) A global comparison signifies that most of the Paleoproterozoic S-type granites were generated by partial melting of Archean crustal rocks.

(7) The new results indicate that the final amalgamation of the northwestern margin of proto-India with other fragments of

Table 4
Compilation of age and Hf-Nd isotopic data of global Paleoproterozoic S-type granites.

Region	Age (Ma)[a]	εHf_t	εNd_t	Hf model age (Ga)	Nd model age (Ga)	Source
India						
Aravalli orogen						
Beawar	1581 ± 24	−10.9 to −8.1	–	2.69–2.84	–	Kaur et al. (2020)
Eastern India						
CGC	1565 ± 27	–	−4.7 to −2.4	–	2.38–3.05	Qasim et al. (2025)
Lesser Himalaya						
Garhwal	1845 ± 19	–	−5.0 to −2.0	–	2.50–2.70	Mishra et al. (2019, 2022)
North China Craton						
Khondalite Belt						
Baotou	2350–2430	−0.01 to +3.9	–	2.76–3.02	–	Shi et al. (2022)
Jining-Liangcheng	1905–1920	−4.4 to +2.0	–	2.57–2.83	–	Shi et al. (2022)
Qianlishan Complex	1949 ± 20	−4.1 to +1.3	−2.9 to −2.8	2.49–2.76	2.67	Li et al. (2022)
Helanshan Complex	1902 ± 22	−0.5 to +1.7	–	2.40–2.48	–	Zhang et al. (2017)
Helanshan Complex	1840–1858	−1.4 to +2.3	–	2.28–2.46	–	Yin et al. (2011)
South China Craton						
Yangtze Block						
Lengshui Complex	1950–2040	−17.1 to −9.7	–	3.22–3.67	–	Li et al. (2021)
Zhongxiang Complex	2000–1930	−17.1 to −9.7	−11.7 to −7.4	3.24–3.67	3.00–3.37	Wang and Dong (2019)
Cathaysia Block						
Wuyishan terrane	1839 ± 16	−8.1 to +2.7	–	2.23–3.03	–	Chen and Xing (2013)
Jinluohou	1878 ± 28	−6.8 to +6.9	−8.5 to −6.7	2.45–3.70	2.90–3.04	Xia et al. (2012)
Siberian Craton						
Tarak massif	1900 ± 10	–	−3.1	–	2.53	Turkina et al. (2006)
Ukrainian Shield						
Bobrovskii Complex	2050–2070	–	+2.1	–	2.33	Savko et al. (2014)
Guyana Shield						
Roraima, Brazil	1962 ± 2	–	–	–	–	Almeida et al. (2007)

[a]: Zircon ages.

Columbia supercontinent took place at ca. 1770 Ma, postdating its time of maximum packing.

CRediT authorship contribution statement

Parampreet Kaur: Writing – review & editing, Writing – original draft, Methodology, Investigation, Funding acquisition, Formal analysis, Conceptualization. **Armin Zeh:** Writing – review & editing, Software, Resources, Methodology, Investigation, Formal analysis. **Naveen Chaudhri:** Writing – review & editing, Writing – original draft, Methodology, Investigation, Formal analysis, Conceptualization. **Prabhakar Dutta:** Methodology, Investigation. **Swati Sharma:** Methodology, Investigation.

Declaration of competing interest

The authors declare that they have no known competing financial interests or personal relationships that could have appeared to influence the work reported in this paper.

Acknowledgements

We thank two anonymous reviewers for their helpful comments and R. Damian Nance for efficient editorial handling. Ministry of Earth Sciences, New Delhi is acknowledged for the financial support (award no. MoES/P.O/(Geo)/100(2)/2017) to carry out this work. AZ thanks A. Gerdes and Linda Markow (FIERCE Frankfurt Germany) for help with Hf isotope analyses.

Appendix A. Supplementary data

Supplementary data to this article can be found online at https://doi.org/10.1016/j.gsf.2025.102182.

References

Abati, J., Aghzer, A.M., Gerdes, A., Ennih, N., 2010. Detrital zircon ages of Neoproterozoic sequences on the Moroccan Anti-Atlas belt. Precambrian. Res. 181, 115–128.
Ahmad, I., Abdul Latheef, T.P., Mondal, M.E.A., Hamidullah, I.S., Parvez, K., 2023. Geochemistry and petrogenesis of the Paleoproterozoic orthogneisses and granitoids of the Banded Gneissic Complex, central Rajasthan, NW India: implications for crustal reworking processes. Acta Geochim. 42, 373–386.
Ahmad, T., Kaulina, T.V., Wanjari, N., Mishra, M.K., Nitkina, E.A., 2009. U-Pb zircon chronology and Sm-Nd isotopic characteristics of the Amgaon and Tirodi Gneissic Complex, Central Indian Shield: constraints on Precambrian crustal evolution. In: Precambrian Continental Growth and Tectonism, 2. Excel India Publishers, New Delhi, pp. 137–138.
Almeida, M.E., Macambira, M.J.B., Oliveria, E.C., 2007. Geochemistry and zircon geochronology of the I-type high-K calc-alkaline and S-type granitoid rocks from southeastern Roraima, Brazil: Orosirian collisional magmatism evidence (1.97–1.96 Ga) in central portion of Guyana Shield. Precambrian Res. 155, 69–97.
Bakliwal, P.C., Ramasamy, S.M., 1987. Lineament fabric of Rajasthan and Gujarat, India. Rec. Geol. Surv. India 113, 54–64.
Barbarin, B., 1999. A review of the relationships between granitoid types, their origins and their geodynamic environments. Lithos 46, 605–626.
Barker, F., 1979. Trondhjemite: definition, environment and hypothesis of origin. In: Barker, F. (Ed.), Trondhjemite, Dacites and Related Rocks. Elsevier, Amsterdam, pp. 1-12.
Barrat, J.A., Zanda, B., Moynier, F., Bollinger, C., Liorzou, C., Bayon, G., 2012. Geochemistry of CI chondrites: major and trace elements, and Cu and Zn isotopes. Geochim. Cosmochim. Acta 83, 79–92.
Bhattacharya, H.N., Mukherjee, A., 2020. A reappraisal of Jharol Formation in the context of stratigraphy of Aravalli Supergroup, Rajasthan, India. J. Earth Syst. Sci. 129, 153.
Bhowmik, S.K., Bernhardt, H.-J., Dasgupta, S., 2010. Grenvillian age high-pressure upper amphibolite-granulite metamorphism in the Aravalli-Delhi mobile belt, northwestern India: new evidence from monazite chemical age and its implication. Precambrian Res. 178, 168–184.
Bradley, D.C., 2011. Secular trends in the geologic record and the supercontinent cycle. Earth-Sci. Rev. 108, 16–33.
Bucholz, C.E., Spencer, C.J., 2019. Strongly peraluminous granites across the Archean–Proterozoic transition. J. Petrol. 60, 1299–1348.
Bucholz, C.E., Stolper, E.M., Eiler, J.M., Breaks, F.W., 2018. A comparison of oxygen fugacities of strongly peraluminous granites across the Archean – Proterozoic boundary. J. Petrol. 59, 2123–2156.

Cawood, P.A., Kröner, A., Collins, W.J., Kusky, T.M., Mooney, W.D., Windley, B.F., 2009. Accretionary orogens through Earth history. In: Cawood, P.A., Kröner, A., (Eds.), Accretionary Systems in Space and Time. Geol. Soc. London Spec. Publ. 318, pp. 1–36.
Cawood, P.A., Hawkesworth, C.J., Dhuime, B., 2013. The continental record and the generation of continental crust. Geol. Soc. Am. Bull. 125, 14–32.
Chappell, B.W., White, A.J.R., 1974. Two contrasting granite types. Pacific Geol. 8, 173–174.
Chappell, B.W., White, A.J.R., 2001. Two contrasting granite types: 25 years later. Aust. J. Earth Sci. 48, 489–499.
Chattopadhyay, N., Gangopadhyay, S., 1984. Petrological study of the ultramafic rocks of Rajasthan. Geol. Surv. India Spec. Publ. 12, 17–24.
Chen, Z.-H., Xing, G.-F., 2013. Petrogenesis of a Palaeoproterozoic S-type granite, central Wuyishan terrane, SE China: implications for early crustal evolution of the Cathaysia Block. Int. Geol. Rev. 55, 1445–1461.
Colleps, C.L., McKenzie, N.R., Sharma, M., Liu, H., Gibson, T.M., Chen, W., Stockli, D.F., 2021. Zircon and apatite U-Pb age constraints from the Bundelkhand craton and Proterozoic strata of central India: insights into craton stabilization and subsequent basin evolution. Precambrian Res. 362, 106286.
Condie, K.C., 1993. Chemical composition and evolution of the upper continental crust: contrasting results from surface samples and shales. Chem. Geol. 104, 1–37.
Condie, K.C., 2011. Earth as an Evolving Planetary System. Elsevier, Amsterdam, p. 574.
Collins, W.J., Richards, S.W., 2008. Geodynamic significance of S-type granite in circum-Pacific orogens. Geology 36, 559–562.
Collins, W.J., Huang, H.-Q., Bowden, P., Kemp, A.I.S. 2020. Repeated S-I-A-type granite trilogy in the Lachlan Orogen, and geochemical contrasts with A-type granites in Nigeria: implications for petrogenesis and tectonic discrimination. In: Janoušek, V., Bonin, B., Collins, W.J., Farina, F., Bowden, P. (Eds.), Post-Archean Granitic Rocks: Petrogenetic Processes and Tectonic Environments. Geol. Soc. London Spec. Publ. 491, 53–76.
Crawford, A.R., 1970. The Precambrian geochronology of Rajasthan and Bundelkhand, northern India. Can. J. Earth Sci. 7, 91–110.
Das, A.R., 1988. Geometry of the superposed deformation in the Delhi Supergroup of rocks, North of Jaipur, Rajasthan. In: Roy, A.B. (Ed.), Precambrian of the Aravalli Mountain, Rajasthan, India. Mem. Geol. Soc. India 7, pp. 247–266.
Dutta, P., Kaur, P., Chaudhri, N., Sharma, S., 2025. Petrogenesis of the Jaisamand sanukitoids and associated TTGs: constraints on the Neoarchean tectonic evolution of the southern Aravalli–Banded Gneissic complex, northwest India. Acta Geochim. 44, 700–730.
Eriksson, P.G., Hattingh, P.J., Altermann, W., 1995. An overview of the geology of Transvaal sequence and Bushveld complex, South Africa. Mineral. Depos. 30, 98–111.
Evans, D.A.D., Mitchell, R.N., 2011. Assembly and breakup of the core of Paleoproterozoic-Mesoproterozoic supercontinent Nuna. Geology 39, 443–446.
Frost, B.R., Frost, C.D., 2008. A geochemical classification for feldspathic igneous rocks. J. Petrol. 49, 1955–1969.
Frost, B.R., Barnes, C.G., Collins, W.J., Arculus, R.J., Ellis, D.J., Frost, C.D., 2001. A geochemical classification for granitic rocks. J. Petrol. 42, 2033–2048.
Gerdes, A., Zeh, A., 2006. Combined U-Pb and Hf isotope LA-(MC-) ICP-MS analyses of detrital zircons: comparison with SHRIMP and new constraints for the provenance and age of an Armorican metasediment in central Germany. Earth Planet. Sci. Lett. 249, 47–61.
Gerdes, A., Zeh, A., 2009. Zircon formation versus zircon alteration – new insights from combined U–Pb and Lu–Hf in-situ LA-ICP-MS analyses, and consequences for the interpretation of Archean zircon from the Central Zone of the Limpopo Belt. Chem. Geol. 261, 230–243.
Gopalan, K., Macdougall, J.D., Roy, A.B., Murali, A.V., 1990. Sm-Nd evidence for 3.3 Ga old rocks in Rajasthan, northwestern India. Precambrian Res. 48, 287–297.
Gupta, S.N., Arora, Y.K., Mathur, R.K., Iqbaluddin, Prasad, B., Sahai, T.N., Sharma, S.B., 1997. The Precambrian geology of the Aravalli region, southern Rajasthan and northeastern Gujarat. Mem. Geol. Surv. India 123, p. 262.
Harris, N.B.W., Pearce, J.A., Tindle, A.G., 1986. Geochemical characteristics of collision-zone magmatism. In: Coward, M.P., Ries, A.C., (Eds.), Collision Tectonics. Geol. Soc. London Spec. Publ. 19, pp. 67–81.
Heron, A.M., 1923. Geology of western Jaipur. Rec. Geol. Surv. India 54, 345–397.
Heron, A.M., 1953. The geology of central Rajputana. Mem. Geol. Surv. India 79, 389.
Hildebrand, R.S., Hoffman, P.F., Bowring, S.A., 2010. The Calderian orogen in Wopmay orogen (1.9 Ga), northwestern Canadian Shield. Geol. Soc. Am. Bull. 122, 794–814.
Hoffman, E.L., 1992. Instrumental neutron activation in geoanalysis. J. Geochem. Explor. 44, 297–319.
Hou, G., Santosh, M., Qian, X., Lister, G.S., Li, J., 2008. Configuration of the late Paleoproterozoic supercontinent Columbia: insights from radiating mafic dyke swarms. Gondwana Res. 14, 395–409.
Iaccheri, L.M., Bagas, L., 2020. Zircon provenances provide paleogeographic constraints on models reconstructing the Paleoproterozoic Columbia supercontinent. Gondwana Res. 82, 254–266.
Johansson, Å., Bingen, B., Huhma, H., Waight, T., Vestergaard, R., Soesoo, A., Skridlaite, G., Krzeminska, E., Shumlyanskyy, L., Holland, M.E., Holm-Denoma, C., Teixeira, W., Faleiros, F.M., Ribeiro, B.V., Jacobs, J., Wang, C., Thomas, R.J., Macey, P.H., Kirkland, C.L., Hartnady, M.I.H., Eglington, B.M., Puetz, S.J., Condie, K.C., 2022. A geochronological review of magmatism along the external margin of Columbia and in the Grenville-age orogens forming the core of Rodinia. Precambrian Res. 371, 106463.
Jung, S., Pfänder, J.A., 2007. Source composition and melting temperatures of orogenic granitoids–constraints form CaO/Na_2O, Al_2O_3/TiO_2 and accessory mineral saturation thermometry. Eur. J. Mineral. 19, 859–870.
Kaur, P., Chaudhri, N., Raczek, I., Kröner, A., Hofmann, A.W., 2009. Record of 1.82 Ga Andean-type continental arc magmatism in NE Rajasthan, India: insights from zircon and Sm-Nd ages, combined with Nd-Sr isotope geochemistry. Gondwana Res. 16, 56–71.
Kaur, P., Zeh, A., Chaudhri, N., Gerdes, A., Okrusch, M., 2011a. Archean to Paleoproterozoic crustal evolution of the Aravalli mountain range, NW India, and its hinterland: the U-Pb and Hf isotope record of detrital zircon. Precambrian Res. 187, 155–164.
Kaur, P., Chaudhri, N., Raczek, I., Kröner, A., Hofmann, A.W., Okrusch, M., 2011b. Zircon ages of late Palaeoproterozoic (ca. 1.72-1.70 Ga) extension-related granitoids in NE Rajasthan, India: regional and tectonic significance. Gondwana Res. 19, 1040–1053.
Kaur, P., Zeh, A., Chaudhri, N., Gerdes, A., Okrusch, M., 2013a. Nature of magmatism and sedimentation at a Columbia active margin: insights from combined U-Pb and Lu-Hf isotope data of detrital zircons from NW India. Gondwana Res. 23, 1040–1052.
Kaur, P., Chaudhri, N., Hofmann, A.W., Raczek, I., Okrusch, M., 2013b. Geochemistry and Sm–Nd geochronology of the metasomatised mafic rocks in the Khetri complex, Rajasthan, NW India: evidence of an Early Cryogenian metasomatic event in the northern Aravalli orogen. J. Asian Earth Sci. 62, 401–413.
Kaur, P., Chaudhri, N., Hofmann, A.W., 2015. New evidence for two sharp replacement fronts during albitization of granitoids from northern Aravalli orogen, northwest India. Int. Geol. Rev. 57, 1660–1685.
Kaur, P., Zeh, A., Chaudhri, N., 2017a. Paleoproterozoic continental arc magmatism, and Neoproterozoic metamorphism in the Aravalli-Delhi orogenic belt, NW India: new constraints from in situ zircon U-Pb-Hf isotope systematics, monazite dating and whole rock geochemistry. J. Asian Earth Sci. 136, 68–88.
Kaur, P., Eliyas, N., Chaudhri, N., 2017b. Record of post-collisional A-type magmatism in the Alwar complex, northern Aravalli orogen, NW India. Curr. Sci. 112, 608–615.
Kaur, P., Zeh, A., Chaudhri, N., Eliyas, N., 2017c. Two distinct sources of 1.73-1.70 Ga A-type granites from the northern Aravalli orogen, NW India: constraints from in situ zircon U-Pb ages and Lu-Hf isotopes. Gondwana Res. 49, 164–181.
Kaur, P., Zeh, A., Chaudhri, N., 2019a. U-Pb age and Hf isotope records of detrital zircon grains from the North Delhi Supergroup, NW India: implications for provenance and stratigraphic correlations. Int. J. Earth Sci. 108, 2683–2697.
Kaur, P., Zeh, A., Chaudhri, N., 2019b. Archean crustal evolution of the Aravalli Banded Gneissic Complex, NW India: constraints from zircon U-Pb ages, Lu-Hf isotope systematics, and whole-rock geochemistry of granitoids. Precambrian Res. 327, 81–102.
Kaur, P., Zeh, A., Chaudhri, N., Tiwana, J.K., 2020. First evidence of late Paleoproterozoic/ early Mesoproterozoic sediment deposition and magmatism in the central Aravalli orogen (NW India). J. Geol. 128, 109–129.
Kaur, P., Zeh, A., Chaudhri, N., 2021. Archean to Proterozoic (3535-900 Ma) crustal evolution of the central Aravalli Banded Gneissic Complex, NW India: new constraints from zircon U-Pb-Hf isotopes and geochemistry. Precambrian Res. 359, 106179.
Kaur, P., Zeh, A., Chaudhri, N., Dutta, P., 2022. Detrital zircon U-Pb-Hf isotope record of conglomerates in the southern Aravalli orogen, NW India: implications for stratigraphy, provenance and Archean to Paleoproterozoic crustal evolution. Precambrian Res. 379, 106800.
Kaur, P., Zeh, A., Chaudhri, N., Sharma, S., 2023a. Neoarchean to Paleoproterozoic crustal evolution of the central Aravalli-Banded Gneissic Complex (NW India): evidence from zircon U-Pb-Hf isotope systematics and whole rock composition of Neoarchean sanukitoids, Paleoproterozoic granitoids and metasedimentary rocks. Precambrian Res. 399, 107236.
Kaur, P., Zeh, A., Chaudhri, N., Manisha, Tiwana, J.K., Dutta, P., 2023b. Stenian sediments (< 1065 Ma) and Tonian A- and I -type magmatism (1000–970 Ma) along the western margin of the central Aravalli orogen, NW India: petrogenetic and geodynamic implications. Gondwana Res. 117, 23–40.
Kaur, P., Zeh, A., Chaudhri, N., Dutta, P., Gerdes, A., 2025. Aravalli A-type granites (ca. 1.72 Ga), NW India: petrogenesis, geodynamic evolution, and global implications for late Paleoproterozoic crustal reworking. Precambrian Res 430, 107936.
Khaksar, T., Rashidnejad-Omran, N., Li, S.-Q., Song, S.-G., Kananian, A., Chen, F., Li, S., 2022. Geochronology and petrogenesis of granitoids and associated mafic enclaves from Ghohroud in the Urumieh-Dokhtar magmatic arc (Iran): evidence for magma mixing during the closure of the Neotethyan ocean. Geol. J. 57, 3313–3332.
Kohn, M.J., Paul, S.K., Corrie, S.L., 2010. The lower Lesser Himalayan sequence: a Paleoproterozoic arc on the northern margin of the Indian plate. Geol. Soc. Am. Bull. 122, 323–335.
Kusky, T.M., Santosh, M., 2009. The Columbia connection in North China. In: Reddy, S.M., Mazumder, R., Evans, D.A.D., Collins, A.S., (Eds.), Palaeoproterozoic Supercontinents and Global Evolution. Geol. Soc. London Spec. Publ. 323, 49–71.
Laurent, O., Martin, H., Moyen, J.-F., Doucelance, R., 2014. The diversity and evolution of late-Archean granitoids: evidence for the onset of "modern-style" plate tectonics between 3.0 and 2.5 Ga. Lithos 205, 208–235.
Li, K., Deng, Q., Wang, J., Yakymchuk, C., Hou, M., Cui, X., Ren, G., Ren, F., Luo, W., 2021. Paleoproterozoic S-type granites in the Lengshui complex, South China: implications for the tectonic evolution of the Yangtze Block. Int. Geol. Rev. 63, 1471–1489.

Li, W., Yin, C., Lin, S., Li, W., Gao, P., Zhang, J., Qian, J., Qiao, H., 2022. Paleoproterozoic tectonic evolution from subduction to collision of the Khondalite Belt in North China: evidence from multiple magmatism in the Qianlishan complex. Precambrian Res. 368, 106471.

Ludwig, K.R., 2012. User's Manual for Isoplot 3.75: a Geochronological Toolkit for Microsoft Excel. Berkeley Geochronology Center, Speical Publication No. 5.

Magni, V., van Hunen, J., Funiciello, F., Faccenna, C., 2012. Numerical models of slab migration in continental collision zones. Solid Earth 3, 293–306.

Mandal, S., Robinson, D.M., Kohn, M.J., Khanal, S., Das, O., Bose, S., 2016. Zircon U-Pb ages and Hf isotopes of the Askot klippe, Kumaun, northwest India: implications for Paleoproterozoic tectonics, basin evolution and associated metallogeny of the northern Indian cratonic margin. Tectonics 35, 965–982.

Maniar, P.D., Piccoli, P.M., 1989. Tectonic discrimination of granitoids. Geol. Soc. Am. Bull. 101, 635–643.

McKenzie, N.R., Hughes, N.C., Myrow, P.M., Banerjee, D.M., Deb, M., Planavsky, N.J., 2013. New age constraints for the Proterozoic Aravalli-Delhi successions of India and their implications. Precambrian Res. 238, 120–128.

Miller, C.F., McDowell, S.M., Mapes, R.W., 2003. Hot and cold granites? Implications of zircon saturation temperatures and preservation of inheritance. Geology 31, 529–532.

Mishra, S., Singh, V.K., Slabunov, A.I., Nainwal, H.C., Singh, P.K., Chaudhary, N., Nainwal, D.C., 2019. Geochemistry and geodynamic setting of Paleoproterozoic granites of Lesser Garhwal Himalaya, India. J. Geosci. Eng. Env. Tech. 4, 28–38.

Mishra, S., Slabunov, A.I., Nainwal, H.C., Singh, V.K., Singh, P.K., Nesterova, N.S., Sevtov, S.A., 2022. Palaeoproterozoic S-type granites from Garhwal Himalaya, NW India: geochemistry, Sm–Nd isotope systematics and tectonic implications. Geol. J. 57, 2443–2463.

Mondal, M.E.A., Raza, A., 2013. Geochemistry of sanukitoid series granitoids from the Neoarchaean Berach granitoid batholith, Aravalli craton, northwestern Indian shield. Curr. Sci. 105, 102–108.

Moyen, J.-F., Martin, H., 2012. Forty years of TTG research. Lithos 148, 312–336.

Nabelek, P.I., 2020. Petrogenesis of leucogranites in collisional orogens. In: Janoušek, V., Bonin, B., Collins, W.J., Farina, F., Bowden, P. (Eds.), Post-Archean Granitic Rocks: Petrogenetic Processes and Tectonic Environments. Geol. Soc. London Spec. Publ. 491, 179–207.

Nance, R.D., Murphy, J.B., Santosh, M., 2014. The supercontinent cycle: a retrospective essay. Gondwana Res. 25, 4–29.

Nance, R.D., Worsley, T.R., Moody, J.B., 1988. The supercontinent cycle. Sci. Am. 259, 72–79.

Ozha, M.K., Mishra, B., Hazarika, P., Jeyagopal, A.V., Yadav, G.S., 2016. EPMA monazite geochronology of the basement and supracrustal rocks within Pur-Banera basin, Rajasthan: evidence of Columbia breakup in northwestern India. J. Asian Earth Sci. 117, 284–303.

Palme, H., O'Neill, H., 2014. Cosmochemical estimates of mantle composition. In: Holland, H.D., Turekian, K.K. (Eds.), Treatise on Geochemistry. second ed. 3. Elsevier, Oxford, pp. 1–39.

Pandit, M.K., Kumar, H., Wang, W., 2021. Geochemistry and geochronology of A-type basement granitoids in the north-central Aravalli Craton: implications on Proterozoic geodynamics of NW Indian Block. Geosci. Front. 12, 101084.

Patiño Douce, A.E., 1999. What do experiments tell us about the relative contributions of crust and mantle to the origin of granitic magmas? In: Castro, A., Fernandez, C., Vigneresse, J.L., (Eds.), Understanding Granites: Integrating New and Classical Techniques. Geol. Soc. London Spec. Publ. 168, 55–75.

Patiño Douce, A.E., Beard, J.S., 1995. Dehydration-melting of biotite gneiss and quartz amphibolite from 3 to 15 kbar. J. Petrol. 36, 707–738.

Pearce, J.A., Harris, N.B.W., Tindle, A.G., 1984. Trace element discrimination diagrams for the tectonic interpretation of granitic rocks. J. Petrol. 25, 956–983.

Phukon, P., 2022. Nature of the northern Indian plate margin during the assembly of supercontinent Columbia: was it a part of a double subduction? Earth-Sci. Rev. 233, 104185.

Qasim, M., Mahapatro, S.N., Ranjan, S., Asokan, A.D., Sarma, D.S., Ram Mohan, M., 2025. Zircon U-Pb age and petrogenetic constraints on granitic magmatism from the southwestern Chhotanagpur Granite Gneiss Complex: implications for Proterozoic crustal growth in the Central India. Precambrian Res. 422, 107783.

Rahaman, M.S., Mondal, M.E.A., 2015. Evolution of continental crust of the Aravalli craton, NW India, during the Neoarchaean–Palaeoproterozoic: evidence from geochemistry of granitoids. Int. Geol. Rev. 57, 1510–1525.

Rickwood, P.C., 1989. Boundary lines within petrologic diagrams which uses oxides of major and minor elements. Lithos 22, 247–263.

Rogers, J.J.W., Santosh, M., 2002. Configuration of Columbia, a Mesoproterozoic supercontinent. Gondwana Res. 5, 5–22.

Rogers, J.J.W., Santosh, M., 2004. Continents and Supercontinents. Oxford University Press, New York, p. 289.

Rogers, J.J.W., Santosh, M., 2009. Tectonics and surface effects of the supercontinent Columbia. Gondwana Res. 15, 373–380.

Roy, A.B., Jakhar, S.R., 2002. Geology of Rajasthan (Northwest India) Precambrian to Recent. Scientific Publishers, Jodhpur, p. 421.

Roy, A.B., Kröner, A., 1996. Single zircon evaporation ages constraining the growth of the Archaean Aravalli craton, northwestern Indian Shield. Geol. Mag. 133, 333–342.

Sarkar, D.P., Ando, J.-I., Das, K., Chattopadhyay, A., Ghosh, G., Shimizu, K., Ohfuji, H., 2020. Serpentinite enigma of Rakhabdev lineament in western India: origin, deformation characterization and tectonic implications. J. Mineral. Petrol. Sci. 115, 216–226.

Savko, K.A., Samsonov, A.V., Larionov, A.N., Larionov, Y.O., Bazikov, N.S., 2014. Paleoproterozoic A- and S- granites in the eastern Voronezh Crystalline Massif: geochronology, petrogenesis, and tectonic setting of origin. Petrology 22, 205–233.

Sen, S., 1981. Proterozoic palaeotectonics in the evolution of crust and location of metalliferous deposits, Rajasthan. Quart. J. Geol. Min. Met. Soc. India 53, 162–185.

Şengör, A.M.C., Natal'in, B.A., 1996. Turkic-type orogeny and its role in the making of the continental crust. Annu. Rev. Earth Planet. Sci. 24, 262–337.

Shekhawat, L.S., Joshi, D.W., Pandit, M.K., 2001. A relook into the status of granitoids and conglomerate in Salumbar-Jaisamand area, southern Rajasthan: implications for the stratigraphy of the Palaeoproterozoic Aravalli fold belt. J. Geol. Soc. India 58, 53–63.

Shi, Q., Xu, Z.-Y., Zhao, G.-C., Ding, D., Lui, G.-W., Zhao, Z.-H., Yu, J.-Y., Li, C., Bai, L.-Q., Wang, Y., Guo, B., Zhang, K., Liu, C.-F., 2022. Anatexis of late Neoarchean-early Paleoproterozoic and late Paleoproterozoic garnet-bearing leucogranite from the Khondalite Belt in the North China Craton. Int. Geol. Rev. 64, 2837–2865.

Singh, S.P., 1988. Sedimentation patterns of the Proterozoic Delhi Supergroup, northeastern Rajasthan, India, and their tectonic implications. Sedi. Geol. 58, 79–94.

Sinha-Roy, S., 1988. Proterozoic Wilson cycles in Rajasthan. In: Roy, A.B. (Ed.), Precambrian of the Aravalli Mountain, Rajasthan, India. Mem. Geol. Soc. India 7, 95–107.

Song, S.-W., Zhu, D.-C., Wang, Q., Cawood, P.A., Zhan, Q.-Y., Li, S.M., Zhang, L.-L., Zhao, Z.-D., 2022. Generation of *syn*-collisional S-type granites in collision zones: an example from the late Triassic Tanggula Batholith in northern Tibet. Gondwana Res. 104, 185–198.

Stevens, G., Villaros, A., Moyen, J.F., 2007. Selective peritectic garnet entrainment as the origin of geochemical diversity in S-type granites. Geology 35, 9–12.

Streckeisen, A., 1976. To each plutonic rock its proper name. Earth-Sci. Rev. 12, 1–33.

Sylvester, P.J., 1998. Post – collisional strongly peraluminous granites. Lithos 45, 29–44.

Tang, M., Wang, X.-L., Shu, X.-J., Wang, D., Yang, T., Gopon, P., 2014. Hafnium isotopic heterogeneity in zircons from granitic rocks: geochemical evaluation and modelling of "zircon effect" in crustal anatexis. Earth Planet. Sci. Lett. 389, 188–199.

Taylor, S.R., McLennan, S.M., 1985. The Continental Crust: its Composition and Evolution. Blackwell, London, p. 312.

Turkina, O.M., Nozhkin, A.D., Bayanova, T.B., 2006. Sources and formation conditions of early Proterozoic granitoids from the southwestern margin of the Siberian Craton. Petrology 14, 262–283.

Upadhyaya, R., Sharma Jr., B.L., Sharma, B.L., Roy, A.B., 1992. Remnants of greenstone sequence from the Archaean rocks of Rajasthan. Curr. Sci. 63, 87–92.

Villaseca, C., Barbero, L., Herreros, V., 1998. A re-examination of the typology of peraluminous granite types in intracontinental orogenic belts. Trans. R. Soc. Edinburgh 89, 113–119.

Wang, K., Dong, S., 2019. New insights into Paleoproterozoic tectonics of the Yangtze Block in the context of early Nuna assembly: possible collisional granitic magmatism in the Zongxiang complex, South China. Precambrian Res. 334, 105452.

Wang, W., Cawood, P.A., Pandit, M.K., Zhou, M.-F., Chen, W.-T., 2017. Zircon U-Pb age and Hf isotope evidence for an Eoarchaean crustal remnant and episodic crustal reworking in response to supercontinent cycles in NW India. J. Geol. Soc. 174, 759–772.

Wang, W., Cawood, P.A., Pandit, M.K., Zhou, M.-F., Zhao, J.-H., 2019. Evolving passive- and active-margin tectonics of the Paleoproterozoic Aravalli Basin, NW India. Geol. Soc. Am. Bull. 131, 426–443.

Watson, E.B., Harrison, T.M., 1983. Zircon saturation revisited: temperature and composition effects in a variety of crustal magma types. Earth Planet. Sci. Lett. 64, 295–304.

Wedepohl, K.H., 1995. The composition of the continental crust. Geochim. Cosmochim. Acta 59, 1217–1232.

Whalen, J.B., Currie, K.L., Chappell, B.W., 1987. A-type granites: geochemical characteristics, discrimination and petrogenesis. Contrib. Mineral. Petrol. 95, 407–419.

White, A.J.R., Chappell, B.W., 1988. Some supracrustal (S-type) granites of the Lachlan Fold Belt. Trans. R. Soc. Edinburgh 79, 169–181.

Wiedenbeck, M., Goswami, J.N., 1994. High precision $^{207}Pb/^{206}Pb$ zircon geochronology using a small ion microprobe. Geochim. Cosmochim. Acta 58, 2135–2141.

Wiedenbeck, M., Goswami, J.N., Roy, A.B., 1996. Stabilization of the Aravalli Craton of northwestern India at 2.5 Ga: an ion-microprobe zircon study. Chem. Geol. 129, 325–340.

Whitney, D.L., Evans, B.W., 2010. Abbreviations for names of rock-forming minerals. Am. Mineral. 95, 185–187.

Xia, Y., Xu, X.-S., Zhu, K.-Y., 2012. Paleoproterozoic S- and A-type granites in southwestern Zhejiang: magmatism, metamorphism and implications for the crustal evolution of the Cathaysia basement. Precambrian Res. 216–219, 177–207.

Yang, X.-M., Drayson, D., Polat, A., 2019. S-type granites in the western Superior province: a marker of Archean collision zones. Can. J. Earth Sci. 56, 1409–1436.

Yin, C., Zhao, G., Guo, J., Sun, M., Xia, X., Zhou, X., Liu, C., 2011. U–Pb and Hf isotopic study of zircons of the Helanshan complex: constrains on the evolution of the Khondalite Belt in the Western Block of the North China Craton. Lithos 122, 25–38.

Zeh, A., Gerdes, A., 2012. U–Pb and Hf isotope record of detrital zircons from gold bearing sediments of the Pietersburg Greenstone Belt (South Africa) – is there a common provenance with the Witwatersrand Basin? Precambrian Res. 204–205, 46–56.
Zhang, D.-H., Wei, J.-H., Fu, L.-B., Schmitt, A.K., Wang, D.-Z., Tan, J., Liu, J.-K., 2017. Petrogenesis and thermal overprint of S-type granites in Helanshan region, North China Craton: constraints on the 1.90 Ga khondalites decompression melting and 1.32 Ga tectono-thermal event. Precambrian Res. 303, 660–672.
Zhang, Q., Liu, Y., Wu, Z., Huang, H., Li, K., Zhou, Q., 2019. Late Triassic granites from the northwestern margin of the Tibetan Plateau, the Dahongliutan example: petrogenesis and tectonic implications for the evolution of the Kangxiwa Palaeotethys. Int. Geol. Rev. 61, 175–194.
Zhao, G., Cawood, P.A., 2012. Precambrian geology of China. Precambrian Res. 222–223, 13–54.
Zhao, G., Cawood, P.A., Wilde, S.A., Sun, M., 2002. Review of global 2.1-1.8 Ga orogens: implications for a pre-Rodinia supercontinent. Earth-Sci. Rev. 59, 125–162.
Zhao, G., Sun, M., Wilde, S.A., Li, S., 2004. A Paleo-Mesoproterozoic supercontinent: assembly, growth and breakup. Earth-Sci. Rev. 67, 91–123.
Zhao, G., Li, S., Sun, M., Wilde, S.A., 2011. Assembly, accretion, and break-up of the Palaeo-Mesoproterozoic Columbia supercontinent: record in the North China Craton revisited. Int. Geol. Rev. 53, 1331–1356.
Zhao, G., Sun, M., Wilde, S.A., Li, S., 2005. Late Archean to Palaeoproterozoic evolution of the North China Craton: key issues revisited. Precambrian Res. 136, 177–202.
Zhu, D.-C., Wang, Q., Zhao, Z.-D., Chung, S.-L., Cawood, P.A., Niu, Y., Liu, S.-A., Wu, F.-Y., Mo, X.-X., 2015. Magmatic record of India-Asia collision. Sci. Rep. 5, 14289.
Zhu, Z., Campbell, I.H., Allen, C.M., Burnham, A.D., 2020. S-type granites: their origin and distribution through time as determined from detrital zircons. Earth. Planet. Sci. Lett. 536, 116140.